AD-A132 511 CERTIFICATE OF APPROVAL(U) AIR FORCE INST OF TECH 1/2
WRIGHT-PATTERSON AFB OH G C GROGAN JUN 83
AFIT/CI/NR-83-18T

UNCLASSIFIED F/G 20/6 NL

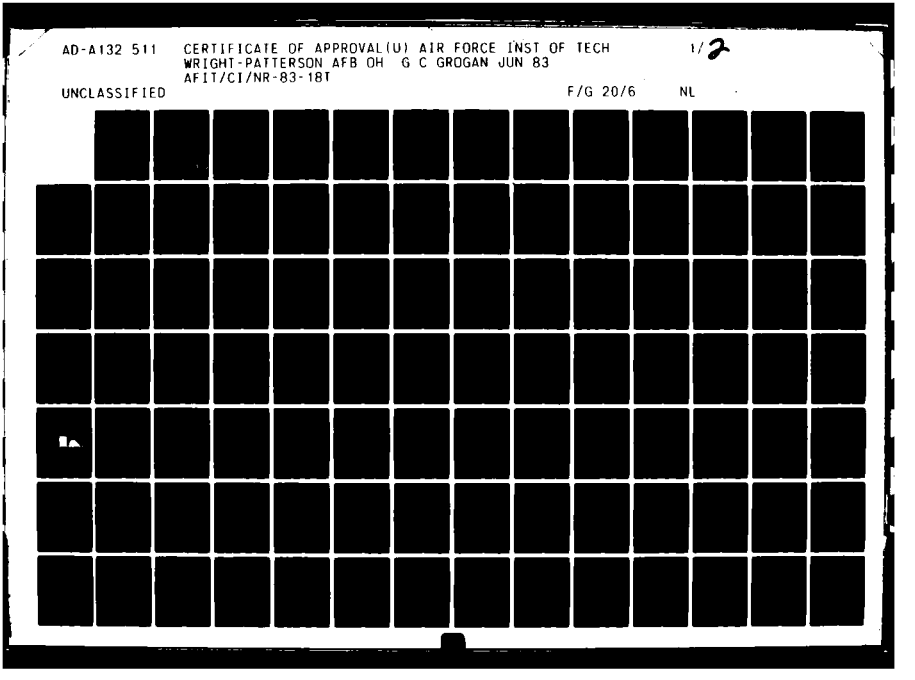

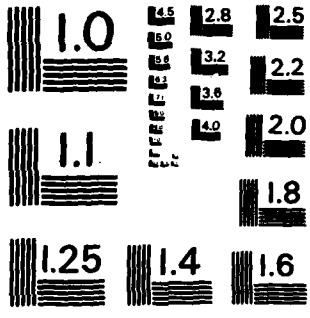

College of Graphic Arts and Photography
Rochester Institute of Technology
Rochester, New York

CERTIFICATE OF APPROVAL

M.S. DEGREE THESIS

The Master's Thesis of George C. Grogan
has been examined and approved
by the thesis committee as satisfactory
for the thesis requirement for the
Master of Science degree

Dr. John R. Schott, Thesis Adviser

Mr. James J. Jakubowski

Major Charles P. Datema

11 June 1983
(Date)

UNCLASS

SECURITY CLASSIFICATION OF THIS PAGE (When Data Entered)

REPORT DOCUMENTATION PAGE		READ INSTRUCTIONS BEFORE COMPLETING FORM
1. REPORT NUMBER AFIT/CI/NR -83-18T	2. GOVT ACCESSION NO. A132577	3. RECIPIENT'S CATALOG NUMBER
4. TITLE (and Subtitle) A Model to Predict the Reflectance from a Concrete Surface as a Function of the Sun-Object-Image Angular Relationship		5. TYPE OF REPORT & PERIOD COVERED THESIS/DISSERTATION 6. PERFORMING ORG. REPORT NUMBER
7. AUTHOR(s) George C. Grogan		8. CONTRACT OR GRANT NUMBER(s)
9. PERFORMING ORGANIZATION NAME AND ADDRESS AFIT STUDENT AT: Rochester Institute of Technology		10. PROGRAM ELEMENT, PROJECT, TASK AREA & WORK UNIT NUMBERS
11. CONTROLLING OFFICE NAME AND ADDRESS AFIT/NR WPAFB OH 45433		12. REPORT DATE 11 June 83 13. NUMBER OF PAGES 95
14. MONITORING AGENCY NAME & ADDRESS(if different from Controlling Office)		15. SECURITY CLASS. (of this report) UNCLASS 15a. DECLASSIFICATION/DOWNGRADING SCHEDULE

16. DISTRIBUTION STATEMENT (of this Report)

APPROVED FOR PUBLIC RELEASE; DISTRIBUTION UNLIMITED

17. DISTRIBUTION STATEMENT (of the abstract entered in Block 20, if different from Report)

Approved for public release: IAW AFR 190-17.
LYNN E. WOLAVER
Dean for Research and Professional Development
Air Force Institute of Technology (ATC)
Wright-Patterson AFB OH 45433

18. SUPPLEMENTARY NOTES

APPROVED FOR PUBLIC RELEASE: IAW AFR 190-17

1 SEP 1983

LYNN E. WOLAVER
Dean for Research and
Professional Development
AFIT, Wright-Patterson AFB OH

19. KEY WORDS (Continue on reverse side if necessary and identify by block number)

20. ABSTRACT (Continue on reverse side if necessary and identify by block number)

ATTACHED

DD FORM 1 JAN 73 1473 EDITION OF 1 NOV 65 IS OBSOLETE UNCLASS

SECURITY CLASSIFICATION OF THIS PAGE (When Data Entered)

A MODEL TO PREDICT THE REFLECTANCE FROM A CONCRETE SURFACE AS A FUNCTION OF THE SUN-OBJECT-IMAGE ANGULAR RELATIONSHIP

by

George C. Grogan

Submitted to the Photographic Science and Instrumentation Division in partial fulfillment of the requirements for the Master of Science degree at the Rochester Institute of Technology

ABSTRACT

A study was made of the variation in the reflectance of a concrete sample as the sun-object-image angular relationship was varied. The research work was performed in the controlled conditions of a laboratory so that atmospheric effects could be neglected. Reflectance measurements were taken from a concrete sample whose surface roughness had been measured. Both specular

and diffuse illumination in the red (630 - 680nm) wavelength region of the visible spectrum were measured. A model which can be used to predict the reflectance value for a given sun-object-image angular relationship was developed. Actual reflectance measurements taken outdoors agreed to within one percent of the model's predicted reflectance values.

83-18T

A MODEL TO PREDICT THE REFLECTANCE FROM A CONCRETE SURFACE AS A FUNCTION OF THE SUN-OBJECT-IMAGE ANGULAR RELATIONSHIP

by

GEORGE C. GROGAN

B.S. UCLA

(1971)

A thesis submitted in partial fulfillment
of the requirements for the degree of
Masters of Science in the School of
Photographic Arts and Sciences in the
College of Graphic Arts and Photography
of the Rochester Institute of Technology

June 1983

Signature of the Author.....
Photographic Science and
Instrumentation Division

Accepted by.....
Coordinator, Graduate Program

ACKNOWLEDGEMENTS

This work would not have been possible without the assistance of the United States Air Force (contract number F33600-75-A-0259). I would like to thank the personnel at the Military Personnel Center and the Air Force Institute of Technology for selecting me for this assignment and supporting me while in Rochester. I would also like to thank my committee members and the faculty and staff at the Rochester Institute of Technology. Finally, a special thanks to Dr. John R. Schott, my thesis adviser, Dr. Ronald Francis, department chairman, and my family.

TABLE OF CONTENTS

LIST OF TABLES

LIST OF FIGURES

INTRODUCTION

To achieve more accurate results, many types of remotely sensed data have corrections applied to them prior to processing. While techniques (Lillesand, 1979) for correcting exposure fall-off and atmospheric attenuation have been developed and refined in recent years, no extensive work on correcting the reflectance value of a target for the sun-object-image angular relationship has been published in the open literature, even though it is known that the reflectance from a target varies with the illumination and viewing angles. Reflectance from a target is very important to an air photo interpreter in the field of remote sensing because it allows him to do many things, including spectral classification and target discrimination. Modifying the value of the reflectance term to account for the sun-object-image angular relationship which existed at the time an image was obtained would allow more accurate image analyses.

Much of the data acquired in remote sensing results from the measurements of reflected solar radiation. Both natural and man-made objects reflect incident solar flux to some extent. The fields of photography, and later remote sensing, have developed around this fact. In figure one, an airborne camera is shown imaging a scene illuminated by both sunlight and skylight. Flux reflected from the target of interest, attenuated by the

atmosphere, and incident upon the film in the camera is labeled α R, where R is the reflectance value of the target. A second source of flux incident upon the film is called airlight, β. Airlight is flux that has been scattered by the atmosphere onto the film without ever reaching the target.

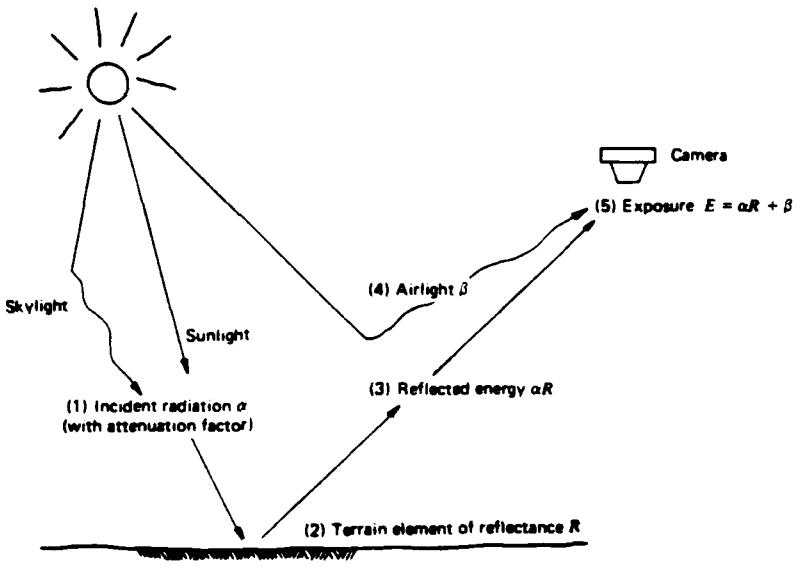

Factors Relating Film Exposure to Ground Reflectance

Figure 1 (Piech and Walker, 1971)

A model (Piech and Walker, 1971) commonly used in remote sensing to relate reflectance to exposure can be stated as follows:

$$E = \alpha R + \beta \qquad (1)$$

where E = total illumination incident on the film at a

given point multiplied by time

α = proportionality factor of the total illumination on the target

R = reflectance of the target

β = airlight (illumination incident on the film at a given point due to atmospheric scattering multiplied by time) other than that reflected from the object.

The linear relationship expressed in Piech and Walker's model may be plotted as in figure two.

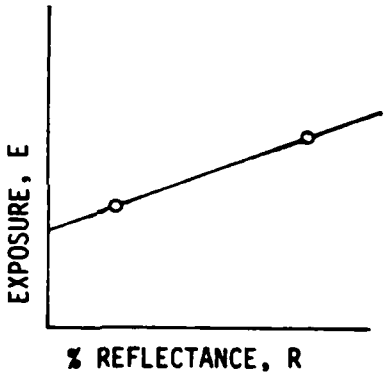

Exposure Versus Reflectance

Figure 2

If the values of E, α, and β can be determined, then the reflectance value for a particular target on a piece of film can be calculated by rearranging equation one:

$$R = \frac{E - \beta}{\alpha} \qquad (2)$$

Techniques for determining the values of E, α, and β are described below.

The exposure value, E, can be determined by selecting a frame of film containing the target's image, measuring the density of the image with a microdensitometer, and then comparing that value to a sensitometric control.

There are several ways to determine the values of α and β. The most accurate would be to place at least two panels of known reflectance in the scene to be imaged. The densities of the panel's images could then be measured with a microdensitometer, and the exposure values necessary to produce those densities could be established. Regressing the two exposure values against the two known reflectance values would produce values for α and β. Unfortunately, this technique is not practical for high altitude-resolution limited remote sensing applications because the panels would have to be huge in order to be resolveable. Building such large-sized panels would be very expensive, and transporting them, even in sections, would be very difficult. This technique would also be impractical for denied access type situations because it would be almost impossible to locate panels in the area to be imaged.

A technique to determine α and β values for a denied access type area (or a remote area where panels could not be located), called the Scene Color Standard, was developed by Piech and Walker in 1972. They were able to determine values for α and β

from an image that contained shadows and any resolveable object (e.g., tennis court, road, parking lot) whose reflectance value was known or could be closely approximated. (According to Schott (1982), objects made from concrete have become the recommended standard and are usually the most commonly selected.) Using the exposure value associated with the density of the imaged object, and the values of α and β calculated by this technique, it is possible to determine a reflectance value for any other object in that image.

A less accurate technique (Schott, 1982) to find α and β is to use two large targets in the image whose reflectances can be closely approximated. Regressing the exposure values against the target's estimated reflectance values will yield approximate values of α and β. A reflectance value for any object in the image can then be determined by substituting the values of α, β, and E into equation (2).

From an intelligence view point, the reflectance value for an unknown object is important because it can be used to help determine the surface material of the object. Knowing the material may help determine what the object is or for what it was designed. Since the reflectance value of a known object is often used to determine values for α and β, a closer examination of the reflectance term is warranted. Slater (1980) has described spectral reflectance, R, as a function of twelve variables.

$$R(\lambda) = R(\lambda, \Delta\lambda; \theta, \phi, \theta', \phi'; d\Omega, d\Omega'; P; \Delta x, \Delta y; t) \qquad (3)$$

where λ = mean wavelength

$\Delta\lambda$ = wavelength bandwidth

θ = angle of incidence of the flux at the surface

ϕ = azimuthal angle of the plane of incidence with respect to a direction across the surface

θ' = angle to the surface normal from which the flux is detected

ϕ' = azimuthal angle of the plane of reflection

$d\Omega$ = solid angle subtended by the source at a point on the surface

$d\Omega'$ = solid angle subtended by the entrance pupil of the sensor at the surface

P = polarization properties of the surface

Δx = dimension of the surface of interest

Δy = dimension of the surface of interest

t = time dependence that relates weather or seasonal changes to surface reflectance

By referencing figure three, it will be noted that the terms θ, θ', ϕ, and ϕ' all involve angles. The interaction between these terms is often referred to as the sun-object-image angular relationship. Varying any one of these angles may produce a change in reflectance. The relationship may be simplified to

three angular terms by combining the difference between the azimuthal angles Φ and Φ' into one angle, ψ. The terms could then be redefined as the illumination angle, θ, measured from

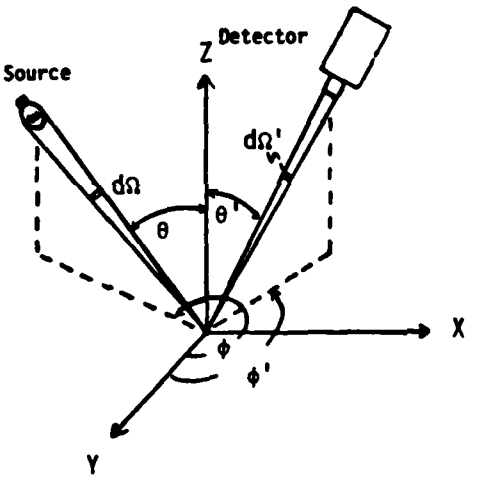

Slater's Angular Relationships

Figure 3

a plane parallel to the surface of the target; the viewing angle, Φ, measured from a plane parallel to the surface of the target; and the azimuth angle, ψ, formed by the vertical planes connecting object to source and object to detector. See figure four.

By holding the other variables in equation (3) constant, and varying θ, Φ, and ψ, it will be possible to determine how reflectance varies as a function of the sun-object-image angular relationship, and to model reflectance as a function of the three angles θ, Φ, and ψ.

For simplicity, Piech and Walker's model assumed that the object imaged was a Lambertian surface (so that the specular components of reflection could be ignored) and that the detector was positioned normal to the object being imaged. While the second assumption would be accurate for high altitude Landsat type imaging, it would not be accurate for a system that had the capability of imaging objects far from the vertical axis. When comparing Landsat images, a user should realize that although

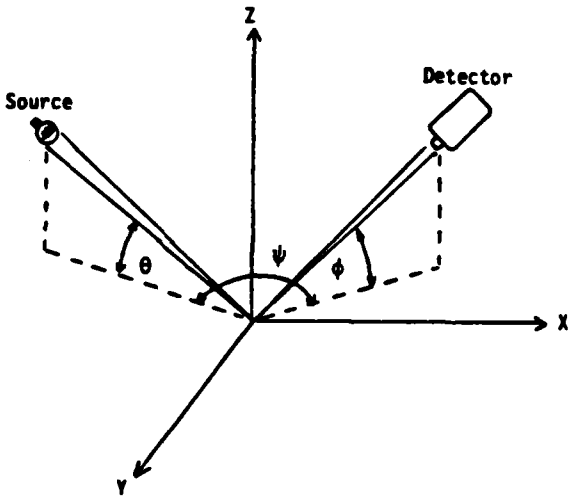

Sun-Object-Image Angular Relationship

Figure 4

the images have essentially a normal viewing angle, the sun and azimuth angles existing when the images were recorded may be quite different. It would be advantageous to be able to account for these angular differences when calculating the mean

reflectance of a target. This would also be important in applications where the mean reflectance value is used in determining the slit width necessary to get the correct exposure on the aerial film of a strip camera. Taking the angular relationship into account when calculating the reflectances of unknown targets by the Scene Color Standard technique should yield more accurate reflectance values for those unknown targets.

As mentioned earlier, targets of known reflectance that are resolveable on high altitude imagery can be used to determine the values of α and β. Two targets which are common to many areas imaged from the air are concrete and asphalt parking lots/roadways. In 1972 two researchers, Egbert and Ulaby, published a study on the reflectance of both asphalt and grass as a function of the sun-object-image angular relationship. Although they measured the reflectance of asphalt as a function of the sun-object-image angular relationship, they did not try to model it. Since no reference to the reflectance of concrete was found during the literature review and since concrete is one of the standards used in the Scene Color Standard technique to calculate values of α and β, its choice as the reflectance target in the study of reflectance variations due to sun-object-image angular variations seemed logical. The reflectance of concrete may vary anywhere from 20 - 35%; when an exact value is unknown, 30% is commonly chosen (Schott, unpublished literature 1982). Selecting 30% when the actual value was 20% would result in an error of 10

reflectance units. Developing a model which could reduce this error to one reflectance unit would be a significant step forward. When a mathematical relationship between reflectance and the involved angles is established, corrections for the sun-object-image angular relationships can be applied to airborne data prior to processing in much the same way that atmospheric and exposure fall-off corrections are applied.

The intent of this thesis project was to model the reflectance of a concrete surface as a function of the sun-object-image angular relationship. To simplify the project it was decided to measure reflectance only in the red portion of the spectrum. If it proved possible to develop a meaningful model, future researchers might then be able to build on this work in an attempt to derive a model that would apply to all concrete surfaces and all visible wavelengths.

LITERATURE SURVEY

Many studies dealing with the reflectance of various targets have been published, but only a limited number of studies tried to account for the sun-object-image angular relationship. Most of these studies dealt with the reflectance of vegetation and did not thoroughly explore the angular relationships involved. Very limited work has been published on mathematically modeling reflectance as a function of the sun-object-image angular relationship, and all of the studies found dealt with vegetation canopies. Although most of the material which follows does not specifically address concrete reflectance measurements, a brief review of the related literature seems relevant.

Using Landsat data, Duggin (1977) studied the variation in reflectance of Australian wheat with solar elevation. He plotted reflectance versus solar elevation for four different Landsat bands and seven varieties of wheat. He then plotted the ratio of bands seven to five against solar elevation; see figure five. Although the sun angles did vary, he was unable to consider varied azimuth angles (less than 0.4 degree change) since his data was from a single date. The viewing angle for all his data was essentially normal. Duggin did not attempt to model the variations observed.

Jackson et al (1979) basically repeated Duggin's work but

used a hand held radiometer to measure reflectance rather than available Landsat data. They measured the spectral reflectance of wheat in the field with varying sun and azimuth angles. They did not vary the viewing angle. Relative reflectance values were calculated by ratioing against a 100% reflectance panel.

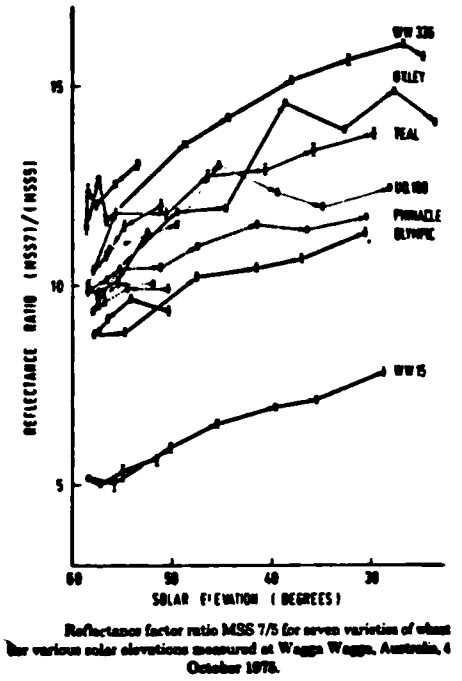

Reflectance factor ratio MSS 7/5 for seven varieties of wheat for various solar elevations measured at Wagga Wagga, Australia, 4 October 1976.

Figure 5 (Duggin, 1977)

They plotted reflectance versus solar elevation for four different bands comparable to Landsat. The ratios of bands seven to five were plotted against solar elevation; see figure six. Like Duggin, they did not attempt to model. Although based on different types of wheat, the graphic results achieved by Jackson et al were very similar in shape to Duggin's.

Smith and Oliver (1974) investigated the effects of two different sun angles on prarie grass reflectance and came up with

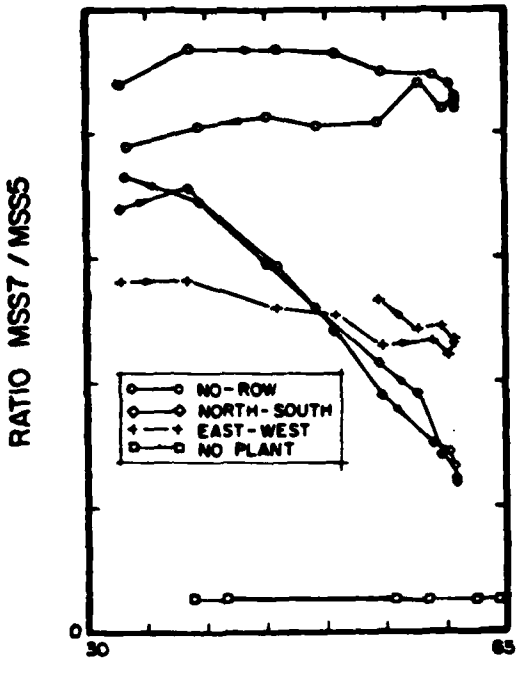

The ratio MSS7/MSS5 as related to solar elevation for a dense no-row plot of wheat for a north-south and an east-west plot at 0.3-m row spacing and for a no-plant plot. The three wheat plots were at the same growth stage.

Fig 6 (Jackson et al, 1979)

a Monte Carlo model to generate sample directional reflectance data for the two simplified solar positions. Their model, which was precise for a normal viewing angle only, was not considered applicable for this study. They treated the direct solar radiation component as a point source whereas the diffuse fraction

was divided into source sectors of the local hemisphere. Results of a feature selection analysis based on their data indicated that different sets of wavelengths were optimum for target discrimination depending on sensor view angle and that the targets may be more easily discriminated for some scan angles than others. They said that agreement of their model was good except for the chlorophyll absorption band.

Breece and Holmes (1971) developed models to account for bidirectional (a consideration of the two angles involved) reflectance of multiple layers of soybean and corn leaves for many different wavelengths. Their work was done in a laboratory, and although they varied the source and viewing angles, they did not vary the azimuth angle. Using a monochromatic beam of light as a source, they gathered 13,680 data points in dealing with the absorptance, transmittance, and reflectance for "m" layers of canopies. Since concrete does not transmit, their model, which accounted for transmission through the canopies, was not applicable to this study.

Suits' (1972) work on multiple leaf reflectance yielded realistic non-Lambertian canopy radiance values. His model for the reflectance from a single layer canopy was of the form:

$$\frac{\pi L}{E_\lambda} \simeq w \left(\frac{1 - e^{z(k+b)}}{k+b} + e^{kz+bz} \right) \rho(\text{soil}) \qquad (4)$$

where w = horizontal projection of the surface area of the leaf

k = horizontal projection of the surface area of the leaf from the viewing angle

b = horizontal projection of the surface area of the leaf from the source angle

e^{kz} = probability of direct detection from a given layer at depth z

z = depth from surface

ρ (soil) = reflectance of the soil beneath the canopy

Welch (1967) investigated the spectral reflectance of five different types of terrain for selected sun and viewing angles. He selected grass, sand, dirt, limestone, and a globe arborvitae to study. He performed his measurements outdoors and did not try to account for illumination variations throughout the day due to atmospheric effects. Welch presented his data in graphical format and did not attempt to model.

Egbert and Ulaby (1972) measured the effects of varied sun-object-image angles on the reflectivity of grass and asphalt, in an attempt to identify which backgrounds contrasted most against roadways. They were looking at the contrast between asphalt roads and grass backgrounds and made no attempt to model, presenting their data in graphical format. See figure seven.

They stated that vertical photography was used for remote sensing missions, and that the standard minimum limit for solar altitude was thirty degrees. This limit was set because

reflectance measurements for sun altitudes greater than thirty degrees were fairly consistent, but measurements taken below thirty degrees tended to be inconsistent. They limited the range

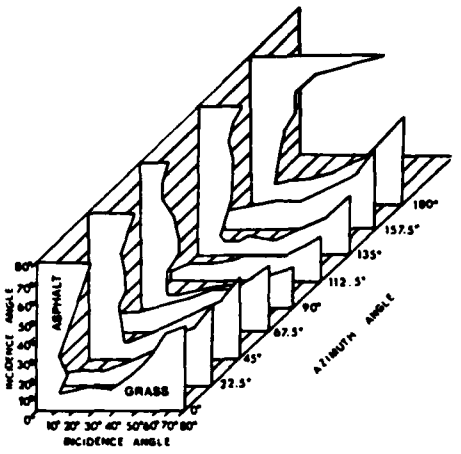

Panchromatic angular variations in reflectance for grass and asphalt at a solar altitude of 15°. This graph is convenient for determining the angles that provide a maximum contrast ratio between a target and the background.

Figure 7 (Egbert and Ulaby, 1972)

of each angle as follows: solar altitude, fifteen to seventy degrees; viewing angle, ten to eighty degrees; and azimuth angle, zero to 180 degrees. They varied the angles in the following increments: solar altitude, ten degrees; viewing angle, ten degrees; and azimuth angle, forty-five degrees. Their measurements of asphalt reflectivity were taken at altitudes of thirty-five to fifty feet and covered the 380 - 900 nm portion of the spectrum in approximately 50 nm increments.

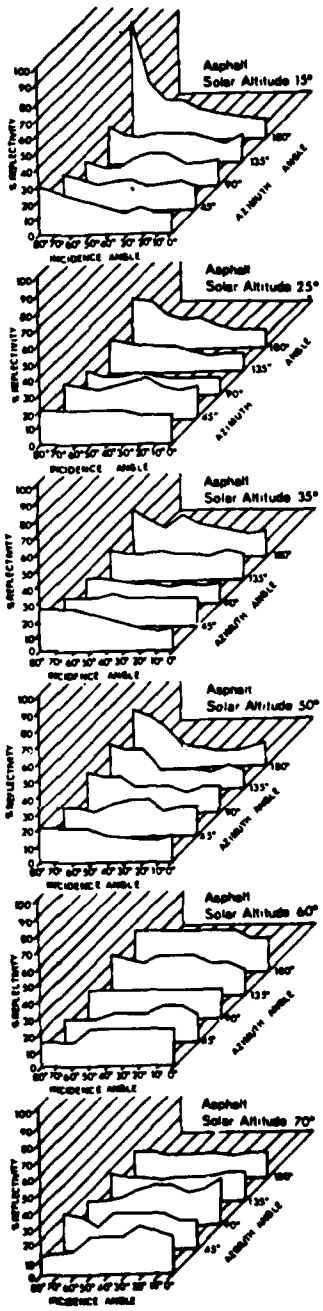

Angular Variation in Asphalt Reflectance

Figure 8 (Egbert and Ulaby, 1972)

They found that variations in reflectance due to changes in the azimuth and incidence angle were greater for grass than for asphalt; see figure eight. The only extreme increase in asphalt reflectivity occurred at a sun angle of fifteen degrees, azimuth angle of 180 degrees, and incidence angle of eighty degrees, and was attributed to the specular component of reflected light.

Besides investigating asphalt rather than concrete, Egbert and Ulaby's work differed from this thesis in at least three other ways. They made their reflectance measurements by ratioing against a single 18% reflectance gray card. They used a different set of Wratten filters, and they did not account for surface roughness. Since Egbert and Ulaby did not model their results, it was not possible to compare the concrete model developed in this experiment to an asphalt model.

Steiner and Haefner (1964) stated that a smooth surface like concrete gives rise to a certain amount of specular reflection. They also stated that most surfaces show a general increase in reflectivity as the detector and source angles (measured from the zenith) increase, no matter what the azimuthal angle.

Since reflectance measurements taken outdoors are a function of the amount of skylight and sunlight incident upon the concrete surface it is necessary to take the atmospheric conditions into account. Measurements taken on an overcast day (small specular

contribution) will not be identical to those taken on a clear sunny day (large specular contribution). Both Lillesand (1979) and Piech and Walker (1971) referred to Hulburt's (1945) work in calculating relative irradiance ratios of sunlight to skylight for different atmospheric conditions; see Table 1.

Table 1

Relative Irradiance Ratios of Sunlight to Skylight for Different Weather Conditions

Weather Condition	Solar/Sky Irradiance
Sunny, clear sky	7:1
Sunny, hazy sky	3:1
Sun through thin clouds	1:1

Palmer (1982) described the problems of using Kodak's Neutral Test Card (18% reflectance gray card) for exacting field work when measuring reflectance. He questioned whether the card departed from being a Lambertian reflector, the card's actual reflectance value, and several other things not pertinent to this study.

Although the reports by Steiner and Haefner (1964) and Egbert and Ulaby (1972) both mentioned concrete, no work was found on the spectral reflectance of concrete as a function of the sun-object-image angular relationship. This study will concentrate on developing a model for a concrete surface that

will, when given the sun, detector, and azimuth angles, yield a specific reflectance value. The model will be developed by combining the results from a regression analysis of specular reflectance data (measured at many different angles) with the diffuse reflectance value from a concrete surface. The results of this study can then be used as a starting point by future researchers to build a model applicable to all concrete surfaces.

THEORY

According to Piech and Walker's model, the illuminance upon a detector can be attributed to three different sources. The α term in the formula $E = \alpha R + \beta$ can be broken down (see appendix A) into two components representing flux from the sun reflecting off the target onto the detector and flux from skylight reflecting off the target onto the detector. The β term accounts for irradiance on the detector due to light scattered by the air column between the detector and target. See figure one and appendix A.

The irradiance on a target due to skylight is assumed diffuse (equal amounts of flux from all directions); therefore, a model which accounts for the reflected skylight components should be independent of viewing angle. A model for the radiance attributable to skylight (from appendix A) is:

$$\frac{E_{sky} R}{\pi} \tag{5}$$

where E_{sky} = irradiance on the target due to skylight

R = percentage diffuse reflectance of the target

It should also be possible to break down the sunlight component into diffuse and specular portions. The radiance attributable to the diffuse portion of the sunlight component can be modeled by:

$$\frac{E_{sun}R}{\pi} \tag{6}$$

where E_{sun} = irradiance of the target due to the diffuse portion of the sunlight

R = percentage diffuse reflectance of the target

The target radiance attributable to the specular portion of the sunlight component is much more difficult to model. It is a function of many things, including viewing angle, source angle, surface roughness, and atmospheric attenuation. It might be modeled by:

$$E_{sun}\, R\, f(\theta,\phi,\psi,r) \tag{7}$$

where E_{sun} = irradiance on the target due to the specular component of sunlight

R = percentage specular reflectance of the target

θ = sun angle

ϕ = detector angle

ψ = azimuth angle

r = surface roughness

According to Schott (1982), another source of target irradiance needs to be considered. In situations where there are surrounding objects (e.g., a building) taller than the target, it is possible for flux to be reflected from the surrounding objects onto the target. Schott has developed a technique for modeling this which takes into account what fraction of the background is composed of tall structures. In order to simplify this experiment, the target was placed on flat terrain with no structures of any significant heigth surrounding it. Since the background did not irradiate the target, it was not an irradiance source during this experiment.

According to Slater (1980), most natural objects exhibit what is referred to as a bidirectional reflectance distributon function. That is, the reflectance distribution from the surface depends on both the direction of the irradiating flux and the direction along which the reflected flux is detected. Slater lists six variables that account for the distribution of flux from a small source. They are the following: 1) the angle of incidence of the flux, 2) the azimuthal angle of the plane of incidence with respect to a direction across the surface, 3) the angle to the surface normal from which the flux is detected, 4) the azimuthal angle of the plane of reflection, 5) the solid

angle subtended by the source at a point on the surface, and 6) the solid angle subtended by the entrance pupil of the sensor at the surface. The first four variables make up the sun-object-image angular relationship.

To understand how the sun, viewing, and azimuth angles can influence a target's reflectance value, it is necessary to take the target's surface into account. Lillesand (1979) states that a target's surface roughness is an important consideration when dealing with reflected flux. He defines a specular reflector as a smooth surface that exhibits mirrorlike reflectance properties (i.e., the angle of reflectance equals the angle of incidence), and a diffuse (Lambertian) reflector as a rough surface that reflects uniformly in all directions. Lillesand goes on to state that most surfaces are neither perfectly specular nor diffuse; see figure nine. He also states that a target can be considered diffuse when its surface height variations are much larger than the wavelength of the incident flux.

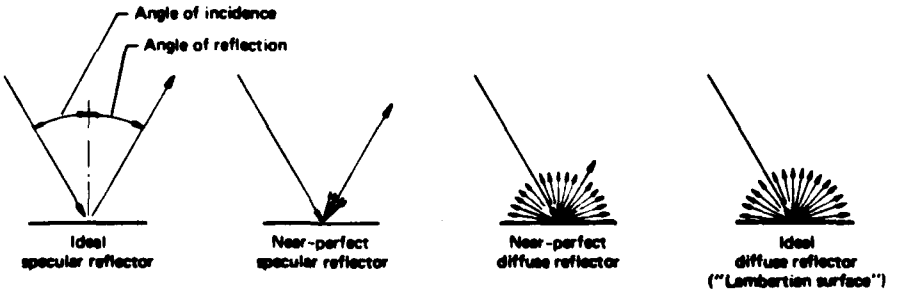

Specular Versus Diffuse Reflectors (Lillesand, 1979)

Figure 9

A concrete surface is much closer to being a near-perfect diffuse reflector than a specular reflector. As the viewing angle is changed, the reflectance value of concrete should be expected to vary over some limited range. (In this experiment the reflectance values varied from 29 - 40%.) This range in reflectance values means that portions of the concrete surface are acting as specular reflectors. (If this was not the case, the reflectance values would have been identical regardless of the angles involved.)

Consider three perfectly specular (on a microscopic level) reflectors which are identical except for surface roughness; see figure ten. A microscopic cross section of each target's surface would show the surfaces to be made up of many tiny ridges and valleys. The greater the distance between the tops of the ridges and the bottom of the valleys, the rougher the surface. Referencing figure ten, the first target is perfectly smooth, having no ridges or valleys. The second target has a fairly smooth surface, and the third target has a rough surface.

Next, let each target be illuminated by the identical point source (similar to the sun). Let an identical detector be positioned above each surface so that the viewing angle is equal to the incidence angle and at an azimuthal angle of 180 degrees.

The perfectly smooth surface would reflect all of the incident flux at the same angle (angle of incidence equals angle of reflectance). Each square unit of the target which was

illuminated would reflect an identical amount of flux, so that if the detector's projected field of view was moved across the surface of the target, no variation in reflectance would be observed.

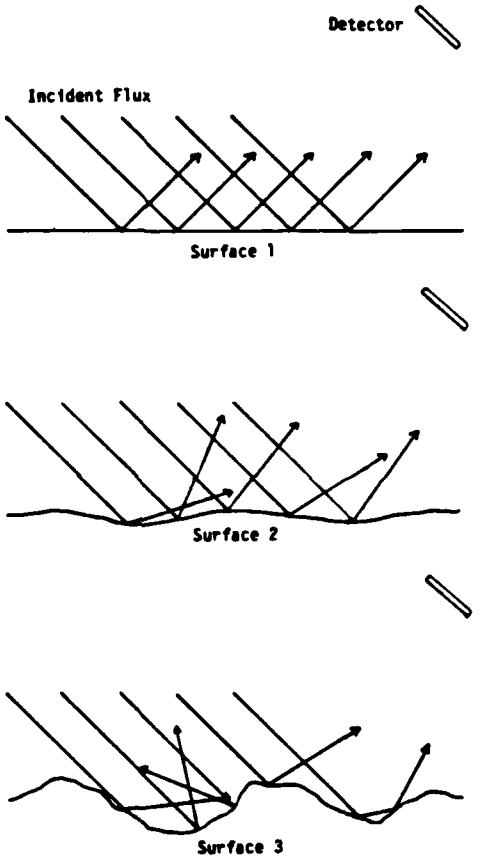

Surface Roughness Effects on Identical Specular Reflectors

Figure 10

The second target's surface is not perfectly smooth, and

different portions of the surface have different slopes. Parallel rays of light incident upon the flux will not necessarily be reflected parallel. Although the angle of reflectance will still equal the angle of incidence, the varied surface slope will cause the flux incident on one area to be reflected at an angle different from the flux reflected by an adjacent area of the surface. The reflected flux is spread over a larger solid angle and not as much of the reflected flux will be incident upon the detector, so the ratio of reflected flux (which is detected) to incident flux will be smaller than for the first target. In other words, the measured reflectance is less. In addition, each square unit of the illuminated target would not necessarily reflect an identical amount of flux (into an identical solid angle) so variations in reflectance would be observed as the detector's projected field of view moved across the surface of the target.

The third target's rough surface has ridges high enough to prevent incident flux from reaching adjoining areas. Since no specular flux is incident upon some of the surface area, it can't be reflected from that area. A visual observer would perceive a shadow. The rougher the surface, the greater the number of shadows. The reflected flux incident upon the detector would be less than for target number two. If the detector's projected field of view was moved across the surface of the target, large variations in illuminance would be detected.

Next, consider three Lambertian (on a microscopic level) reflectors of varying surface roughnesses, each illuminated by a point source located above the surface on a path normal to the surface; see figure eleven. Although all three surfaces are perfect reflectors on a microscopic level, the reflected flux

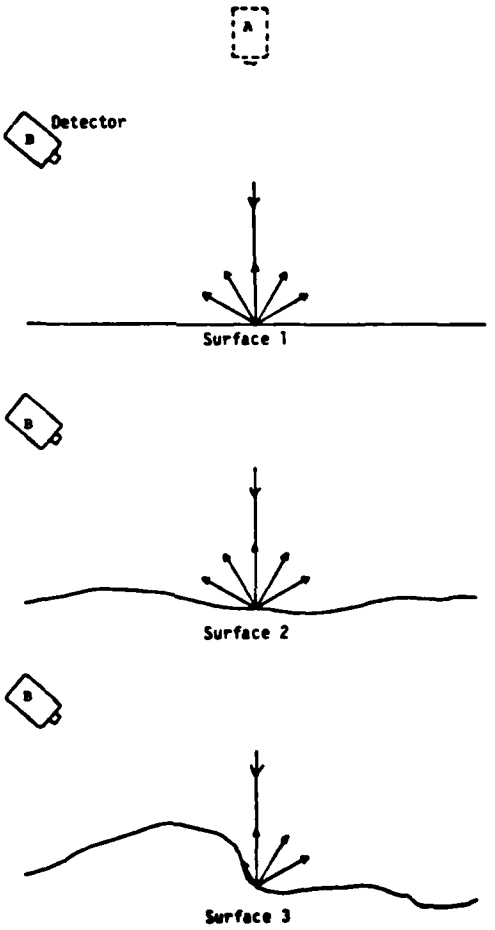

Surface Roughness Effects on Identical Lambertian Reflectors

Figure 11

detected would not be identical when considering the macroscopic level. Tall ridges could block the detector's line of sight and thus decrease the amount of flux detected.

A detector positioned above the perfectly smooth surface (surface one) would detect the same amount of reflected flux no matter what the viewing angle. The amount of reflected flux detected above surface two would also remain constant for different viewing angles, providing the viewing angle of the detector did not approach the horizon (where small ridges might block the detector's line of sight).

If the detector above surface three was rotated from a 90 degree (detector position A) to a 40 degree viewing angle (position B), less reflected flux would be detected, as illustrated. This would happen when the height of the ridges actually obscured the detector's field of view.

For all these cases, the above arguments would be just as applicable if the detector was maintained at a constant viewing angle and the source angle was allowed to vary. The azimuth angle must also be considered because of texture variations in the z direction across the surface.

It is recognized that there is a large (typically from 20 to 35 percent) variation in the reflectance values of different concrete surfaces. As described earlier, Slater (1980) listed the factors that cause this variation in reflectance as follows:

$$R(\lambda) = R(\lambda, \Delta\lambda; \theta, \theta', \phi, \phi'; d\Omega, d\Omega'; P; \Delta x, \Delta y; t). \quad (3)$$

By combining the azimuthal angles as described in the introduction, this can be simplified to:

$$R(\lambda) = R(\lambda, \Delta\lambda; \theta, \phi, \psi; d\Omega, d\Omega'; P; \Delta x, \Delta y; t). \quad (8)$$

By holding all the other variables constant, it was possible to restrict variations in reflectance to a function of just sun-object-image (θ, ϕ, ψ) angular variations.

$$R(\lambda) = R(\theta, \phi, \psi) \quad (9)$$

Techniques for keeping the other variables constant will be described.

According to Slater the shape of the bidirectional reflectance distribution function does not change substantially with wavelength, vegetation being a notable exception. Rather, the overall distribution rises and falls as the reflected wavelength measured is varied. In this experiment the wavelengths reaching the detector were held constant by filters positioned in front of the detector. The red (630-680 nm) wavelengths were selected for this study because radiation in the red portion of the visible spectrum penetrates the atmosphere better than radiation in the blue portion (i.e., Rayleigh scattering is reduced).

The effect of increasing the wavelength interval, $\Delta\lambda$, is to smooth the shape of the bidirectional reflectance distribution function (Slater 1980). The wavelength interval was kept constant by using two filters (a red stacked with an infrared cut-off) which passed a specific bandwidth to the detector. The filters selected for use in this experiment pass a wavelength interval to which color film is sensitive.

The effect of increasing the solid angles, $d\Omega$ and $d\Omega'$, subtended by the source and detector respectively, is to smooth the shape of the bidirectional reflectance distribution function. This is to be expected since a larger solid angle allows flux to either be distributed over a larger area or to be collected from a larger area. Both increases would tend to obscure point variations. The size of the solid angles did not change because no changes were made to the optical systems of either the source or detector after the experiment began. Varying the position of either the source or the detector in order to take measurements did not effect the size of the solid angles. Large arches were constructed so that the projected spot sizes from the detector and source would be large; and, consequently the flux would be integrated over as large a surface area as possible, minimizing the fluctuations in reflectance measurements due to minor surface texture variations.

Polarization properties of the detector could cause errors in the interpretation of detected reflectance variations. If the

remote sensor acted as a polarizer, the flux reaching the detector would also be a function of the orientation of the detector's optical system. Reflectance variations after sun-object-image angular changes might be due to polarization properties of the sensor rather than angular variations.

All surfaces polarize the reflected flux to some extent. According to Slater (1980), near-Lambertian surfaces do not impart much polarization. The smoother the surface, the more specular the reflection and the greater the degree of polarization imparted at reflection. Because of its rough texture, a concrete surface was not expected to impart much polarization. As described in the results, polarization-induced error turned out to be negligible, so no corrections were necessary.

If the surface dimensions ($\Delta x, \Delta y$) of the object to be imaged are less than the projected field of view on the ground, then the flux reaching the sensor would include both that reflected from the object and the background. To insure that only flux reflected by the target reached the detector, the size of the target must be larger than the size of the projected fields of view from both the source and detector. In this experiment the concrete sample's surface area was much greater than the size of the projected fields of view so that target size was not a factor.

The term "t" is the time dependence that relates weather or seasonal changes to the reflectance of the surface. An aged or

weathered surface would have different reflective properties than a new one. A concrete surface covered with snow or water would certainly have different spectral reflectance values compared to a dry, sunlit surface. Because the experiment was conducted indoors, and the detector was only five feet from the target surface, Schott's (1979) technique of assuming atmospheric effects to be negligible was used. Since this research project was conducted in a lab research room, "t" was constant.

Sunlight was simulated with a tungsten-halogen lamp. Although its color temperature (2950°K) was not as hot as the sun's (5900°K), a tungsten-halogen lamp's spectral distribution has a shape very similar to that of the sun's, only shifted to the right. The area of the sample illuminated by the lamp's projected field of view was checked to insure that the illumination across the spot was as uniform as possible; see appendix G.

Lillesand (1979) describes two geommetric effects that can influence the apparent reflectance detected from a surface as the surface texture changes. They are differential shading, and specular reflection. Differential shading is illustrated in figure 12. As shown, the side of the ridges illuminated by the source will reflect more flux than the sides which do not receive direct illumination. For certain surfaces and particular illumination and viewing angles, there can be a wide range in reflectance values.

Lillesand stated that differential shading was a function

of target height and solar elevation and was exacerbated at low sun angles. He goes on to state that variations in slope and slope orientation increase the effect of differential shading. In this experiment illumination angles below thirty degrees were avoided and target heights were not a factor on the macroscopic level.

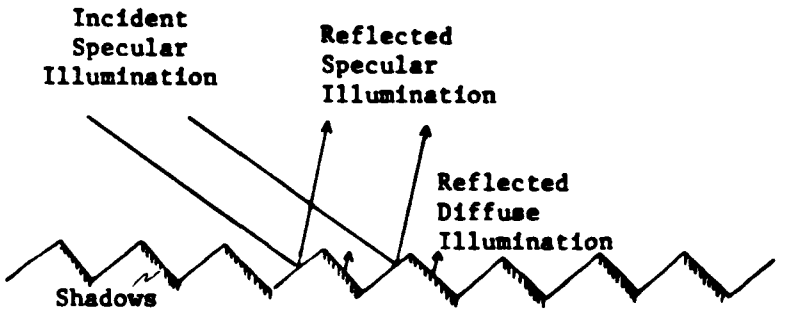

Differential Shading

Figure 12

One of the main objectives of this thesis was to try and account for the specular reflectance. In this experiment the surface texture of the concrete sample was made as uniform as possible so that some areas would not contribute more specular reflectance effects than others. Texture uniformity across the surface, not smoothness, was the main criteria in preparing the surface of the concrete sample to be investigated.

By following the procedures described in this section it was

possible to keep nine of Slater's twelve variables constant and to isolate changes in the reflectance of concrete to changes in either the source angle, azimuth angle, or detector angle:

$$R = f(\theta, \phi, \psi) \tag{10}$$

EXPERIMENTAL PROCEDURE

To model the reflectance from the surface of a concrete sample as a function of the sun-object-image angular relationship, it was necessary to have the capability of accurately measuring reflectance from specific locations throughout a hemisphere. The basic idea behind the experimental procedure was to measure flux from a source that had been reflected by the surface of a concrete sample onto a detector; see figure 13.

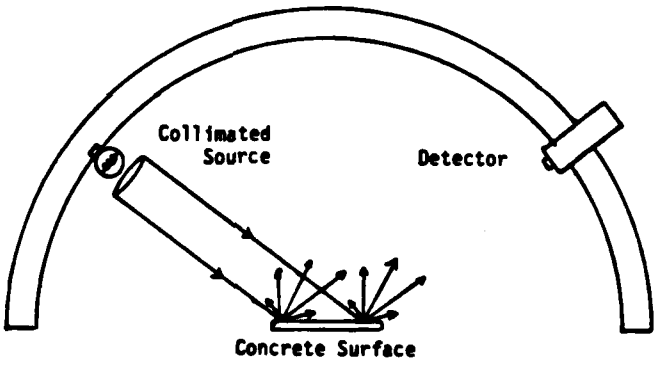

Measuring Specularly Reflected Flux

Figure 13

Specifically, the reflectance measurements required designing and constructing a simple goniophotometer to support the collimated light source and a silicon cell detector filtered

around 650 nm. In addition, reflectance panels of known values were constructed and were used as standards to calibrate the detector signal displayed on a multimeter as voltage. This calibration involved calculating reflectance percentage for the concrete surface by comparing the voltages resulting from the known reflectance of the panels with the voltage resulting from the concrete surface.

To simulate field conditions (Egbert and Ulaby, 1972) a limit of 60 degrees from the zenith was established for the source and detector angles. The cheapest and easiest device to construct to support the source and detector consisted of two 180 degree arches, one to support and position the source, and the other to support and position the detector; see figure 14. A third arch was necessary to provide stability when the azimuth angle between the arches supporting the source and detector approached zero degrees. The arches were cut from a 4' by 8' by 3/4" compressed wood panel. Patterns were laid out and cut so that the outside arch had a diameter of slightly less than ten feet. A hole was drilled vertically through the 90 degree point of each arch. A steel rod, threaded at each end, was placed through the hole in each arch. The rod connected the arches to one another and provided a pivot point about which the arches could be rotated; therefore, the azimuth angle (between the detector and source) could be set at various known angles.

When spread out, the assembled arches formed a hemisphere.

A plum line was hung from the metal rod, and the position of the arches adjusted so that the zenith (90 degree point) of the arches was centered over the origin of a compass card marked on the floor. Compass markings, in ten degree intervals, were

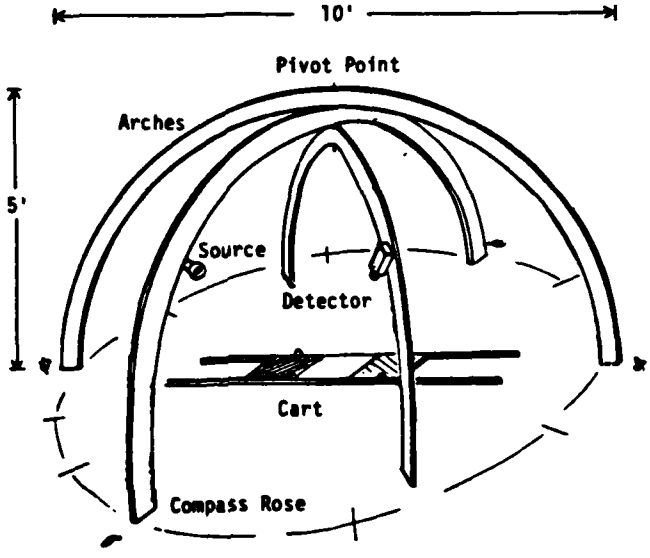

Set-up to Measure Specular Reflectance

Figure 14

placed on the circumference of the arc circumscribed by the arches as they were rotated 360 degrees. Each arch was marked, drilled, and labeled at ten degree intervals to allow for mounting of the detector and source. The holes drilled through the sides of each arch allowed placing the detector and source at precise locations along each arch; see figure 15. By moving either the source or detector along its respective arch, the

position of each could be set accurately and recorded. By rotating the arches relative to one another, the azimuth angle between the source and detector could also be set accurately and recorded.

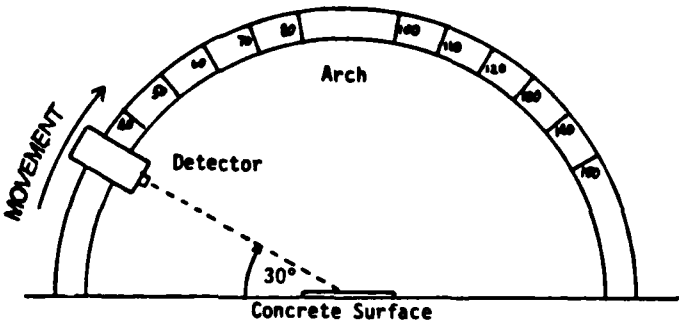

Detector Positions Along Arch

Figure 15

To measure specular reflectance accurately it was necessary to produce parallel light rays; the best way to do that with a non-point source was to collimate the flux. By combining a fresnel lens, a movie camera lens, and a light bulb in a lamp housing from an Ansco microdensitometer, it was possible to produce an acceptably collimated source; see figure 16.

The fresnel lens was selected because it had two desired characteristics, a short focal length and a diameter large enough to produce an acceptably-wide projected spot size on the concrete sample. The assembled light source produced a field

angle of zero degrees and a projected normal field of view diameter of five and one-eighth inches. The movie camera lens was selected because it was the only lens available that had a diameter of better than one inch (to match the lamp housing aperture) and a focal length of less than one and a half inches.

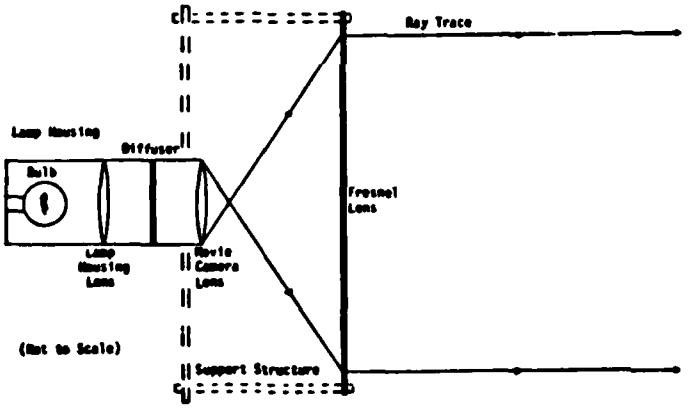

Collimated Light Source

Figure 16

Obtaining lenses with short focal lengths was necessary to keep the overall size of the assembled source reasonably small. The movie camera lens had a very short focal length that produced an image of the source right behind the lens. To insure collimation, the exact distances between lens elements and light source were determined on an optical bench. Mounting the fresnel lens precisely one focal length from the image of the light bulb formed by the camera lens allowed the fresnel lens to image the

filament of the bulb at infinity, effectively making a collimated source. A piece of opal glass was cut to shape and mounted between the bulb and the movie camera lens to diffuse the illumination incident upon the lens. This produced a near uniform illumination across the projected spot size (appendix B). Parts to firmly position each lens relative to the rest of the system were designed and built.

A GE light bulb, stock number 1763, was mounted inside the lamp housing. The bulb was wired to an ammeter which permitted the input current to be monitored. The ammeter was connected to a rheostat that was used to vary the input current, and hence the intensity of the bulb. The rheostat was connected to a step down transformer to allow line voltage from the laboratory room to power the 6 volt bulb.

The assembled light source was bolted through the side of the arch where it could be tightened securely after alignment. Aligning the source was accomplished by placing a piece of transparent plastic with two crosshairs drawn upon it over the fresnel lens and centering the projected crosshairs on the origin of the compass card beneath the arches.

A Spectra Spotmeter was chosen to be the detector. Measurement repeatability was verified by placing the sample and panels at the nadir, under the projected fields of view and taking at least thirty sets of measurements. This process was repeated at four different detector-azimuth-source positions,

each having a different angular relationship. After the initial run of measurements were taken, it was discovered that the variance in repeated measurements was too large in relation to the total variation in reflectance caused by changes in the angular relationships. The photo multiplier tube was removed from the detector housing and replaced with a silicon cell detector. One of the nice features of the Spotmeter was a through-the-lens sighting system for aligning the spot to be measured. By installing a bifurcating mirror the manufacturer made it easy for a user to aim the detector. The first folding mirror had a hole drilled through it permitting flux reflected from the target to reach the detector; see figure 17.

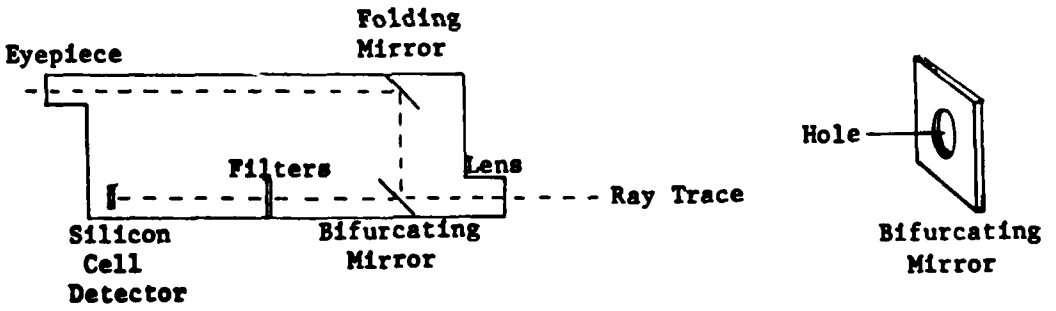

Detector and Bifurcating Mirror

Figure 17

The mirror was interchangeable with other mirrors having holes of various diameters, a feature which allowed the user to

vary the area of the projected field of view. The projected spot size needed to be large enough to integrate the flux over as much surface area as possible (to minimize the effects of surface texture variations) yet small enough that it would never exceed the source's projected spot size. A two inch diameter normal projected spot size was thought to be optimum.

Unfortunately, when the detector was mounted on the arch, none of the mirrors provided by the manufacturer had a hole large enough to provide the desired projected spot size. A replacement mirror was made by sanding and polishing a piece of aluminum, and then drilling it with a bit that provided a 2.1 inch normal projected spot-size (a 2.5 degree field of view) when the detector was mounted at the arch zenith.

Because the bulb used as a source emitted radiation over an approximate wavelength range of 100 to 10,000 nm, it was necessary to filter out all radiation other than that desired (650 nm), so only radiation from the red portion of the visible spectrum could be passed to the detector. The neutral density filter wheel was removed from the detector housing, and one of the neutral density filters was removed and replaced with a number 92 Kodak Wratten filter. The Wratten filter was stacked with a Kodak 301A infrared cutoff filter to transmit only 630 - 680 nm wavelength (measured at 50% transmittance) radiation; see figure 18. Unfortunately, the effort was not entirely successful, for though the Wratten filter prevented shorter wavelength radiation

from passing, the 301A filter did not cut off all the infrared radiation. Radiation in the 980 - 1100 nm wavelength region (measured at 50% transmittance) was passed to the detector, which was sensitive to radiation extending out to 1100 nm, see figure 19. The solution to the unwanted wavelengths was a cold mirror which would block the infrared radiation, but the Institute did not possess one and thesis budget constraints prevented purchasing one. Consequently, it was necessary to accept the detection of infrared radiation.

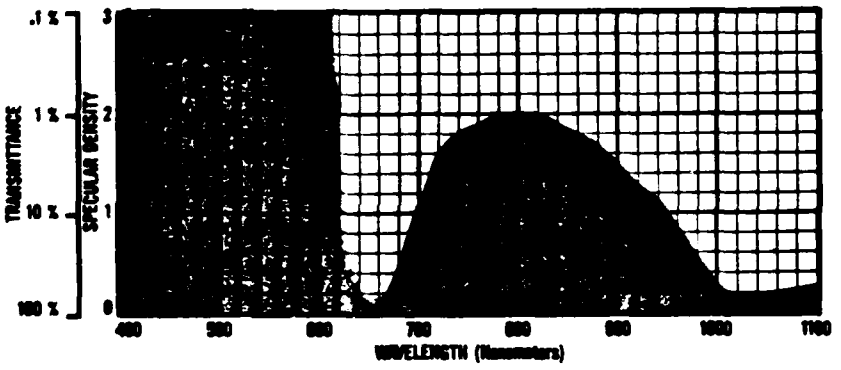

Wavelengths Transmitted by Stacked Filters

Figure 18

The output from the silicon cell detector was run into an amplifier and then passed into a Hewlett-Packard multimeter. The multimeter was placed in an automatic mode which measured voltage. By keeping the current to the source low enough, the

display on the multimeter could be read to three decimal places. The third decimal place provided the precision necessary to get the detector variance down to approximately 0.2% reflectance.

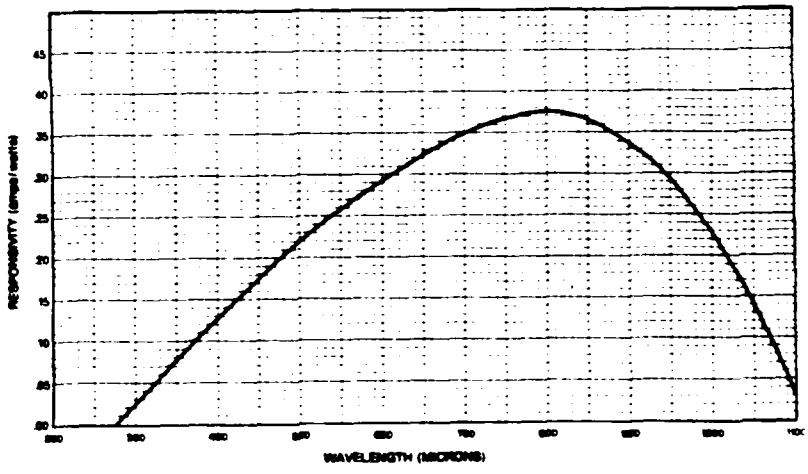

Typical Spectral Response for Detector

Figure 19

Six reflectance panels were made to verify that the detector had a linear response and to get a relative measure of reflectance from the concrete sample. Since the reflectance measurements were going to be made from many different positions, the surfaces of the panels had to be made as near-Lambertian as possible. Six two-foot square panels were cut from a piece of hardboard. The top surface of each panel was then coated with an adhesive spray and covered with fine particle sand. The adhesive bonded a thin layer of sand to the hardboard. Small

bottles were filled with various shades of gray paint produced by combining flat dark gray and flat white auto primer paints. The panels were transported to a spray booth in the physical plant building where a professional-quality spray gun was used to apply the paint uniformly. Five panels were painted with the various shades of gray, and the sixth panel was painted with a white near 100% reflectance paint, Kodak catalog number 6080.

After drying, the panels were cut into several eight inch squares, and one 1" square piece from each color was cut out and measured in a Beckman DK-2A Spectrophotometer. Both the total (diffuse plus specular) and diffuse reflectance of each panel from 400-800 nm were measured; see appendix C. The difference between the total and diffuse components equaled the specular component. Since the difference was negligible, there was essentially no specular component. This was an indication that it was reasonable to assume that all six of the panels were very close to being Lambertian reflectors. Absolute reflectance values (measured at 650 nm) for each panel were determined by the relative ratios of the panel results to the results from a standard reflectance material (barium sulfate). The calculated red reflectance values for the six panels were 16%, 26%, 30%, 56%, 73%, and 94%. The 16% and 56% panels were chosen to bracket the concrete sample since the surface had an expected reflectance value between 20 and 35%.

The detector was proven to have a linear response by

measuring the flux reflected from the panels five different times and statistically analyzing the results; see appendix D.

Six concrete samples were initially prepared, each in an eight inch square, three-fourth inch deep wooden frame. The samples were made from a bag of ready-mix concrete without gravel. A mixture without gravel was selected to eliminate the possibility of specular reflectance from gravel that might be on the surface of the sample. Each sample's surface was finished differently in order to have six surfaces of varying roughness. Texture smoothing was achieved by adding more water to the mixture and then vertically tamping; a trowel and whisk broom were used to increase texture roughness. After the concrete in all six samples had dried, a visual inspection was made and the sample that was visually the most uniform in texture was selected to be evaluated. The sample was arbitrarily named concrete sample one, C1.

Precise positioning of the projected fields of view of both the detector and source minimized the error resulting from surface texture variation by insuring that the same surface area was within the projected field of view each time. It was thought that the same surface area of each of the panels and the sample must be within the projected fields of view of both the detector and source each time a measurement was taken to negate the effects of surface variations across the sample or panels and to guarantee repeatable results. This consideration turned out to

be less important for the reflectance panels since their surfaces were extremely uniform (appendix E).

Measurements were made by placing the panels and sample at the nadir of the arches, one at a time. Because the sample and panels were going to be placed at the nadir so many times, and precise positioning of the projected fields of view was desired, a cart and track system was designed and built. This system made it easy to position the sample or panels in the same location each time, thus standardizing their positions (to within one-eigth of an inch) for the measurements in order to minimize the variance in data caused by imprecise repetitive positioning. The panels and samples were mounted on a cart which was placed on a track permitting movement in only one direction. They were mounted in the following order: 16%, C1, and 56%; see figure 20.

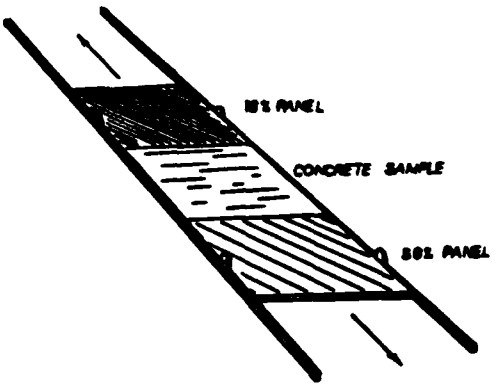

Cart, Concrete Sample, and Reflectance Panels

Figure 20

The cart was pushed back and forth along the track to position the center of the appropriate panel at the nadir. Precise positioning of the cart was accomplished by stopping it when it was aligned with indicator marks placed on the floor. A crosshair was placed on the cart to facilitate alignment of the detector and source. When the appropriate target was at the nadir, the distance from its surface to the pivot point of the arches was identical to that of the other targets when they were at the nadir; this assured the spot size projected by both the source and detector would remain constant and not be a variable.

To simplify the recording of data during this experiment, the term DAS was coined. It is an acronym for the specific Detector angle, Azimuth angle, and Source angle which existed when a particular measurement was taken. As illustrated in figure four, the sun-object-image angular relationship at any particular time can be described by the three angles θ, Φ, and ψ, where θ and Φ are measured from the horizontal. Thus the term DAS 30-150-40 refers to the specific sun-object-image angular relationship where the detector is positioned at an angle of thirty degrees from the horizontal (60 degrees from the normal); the azimuth angle formed by the arches supporting the detector and source is set at 150 degrees; and the light source is positioned at an angle of forty degrees from the horizontal (50 degrees from the normal). See figure 21.

The term DAS XX-30-50 refers to a set of data in which the detector angle was varied while the azimuth and source angle were held constant at thirty and fifty degrees, respectively. Throughout the remainder of this report, a specific sun-object-image angular relationship may be referred to by the term DAS followed by a set of numbers.

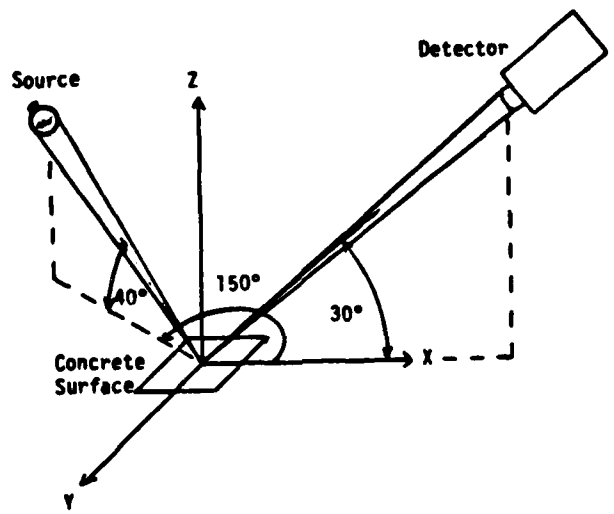

DAS 30-150-40 Angular Relationship

Figure 21

If the measurement equipment (source and detector) had been completely stable, and if the reflectance panels had been perfect Lambertian reflectors, one reflectance measurement from each of the panels would have sufficed, since a Lambertian reflector would have reflected an identical amount of flux in all

directions. For these studies, detector drift required measuring the flux reflected from the concrete sample and the flux reflected from each of the two known panels within thirty seconds of elapsed time. (Taking the measurements in such a short time span minimized the drift error.) This process essentially involved a calibration of the detector for each series of measurements. This calibration also served to minimize any error from line voltage fluctuations or lamp aging.

Since the detector's response was linear, a linear equation which related measured voltage to reflectance could be derived by regressing the experimentally determined voltages (displayed on the multimeter) for each panel against their known reflectance values. Substituting the voltage measured (a function of the reflected flux) when the concrete sample was being checked, into the linear equation and solving, yielded a reflectance value for the sample at that particular sun-object-image angular relationship. The linear equation was valid only for that particular DAS position since the detector's response drifted slowly with time.

Because the regression equation was valid only for one DAS position, it was necessary to repeat the technique at each DAS position that a reflectance value was desired. It was determined earlier that the DAS measurements would be made by varying the three independent variables (angles) separately. The azimuth angle between the detector and source would be varied in 30 degree increments from 0 to 180 degrees. The detector would be

moved across its arch in ten degree increments from 30 to 150 degrees. The source would be moved across its arch in ten degree increments from 30 to 90 degrees.

Three replicate measurements would be made at each DAS position. At some positions (such as DAS 30-0-30) it was physically impossible to take any measurements because the source and detector would have had to be colocated.

To keep the measurements down to a manageable number, the source was not moved from 90 to 150 degrees, nor was the azimuth angle varied from 180 to 360 degrees. Geometrical symmetry nullified the requirement for measuring reflectance at symmetrical DAS positions. This was the same technique used by Egbert and Ulaby (1972). A confirmation of azimuthal symmetry was made by taking replicate measurements at four symmetrical positions and statistically comparing the results (appendix G).

The first measurements were taken at DAS 30-0-40. The 16% reflectance panel was placed at the nadir, and the voltage displayed was recorded. The 16% reflectance panel was then removed and replaced by the concrete sample, C1, and the voltage display recorded. C1 was then removed and replaced by the 56% reflectance panel and the voltage recorded. This process was repeated three times, so that a total of nine measurements at each DAS position were taken.

After the ninth measurement at the DAS 30-0-40 position was taken, the angular relationship was changed and the process

repeated. Measurements were taken in data sets using a constant source angle. The process of changing the angular relationship in an orderly manner continued until all of the 504 possible positions had been evaluated. The measurement process was carried out first by increasing the azimuth angle in 30 degree increments until all of the azimuth angles had been evaluated; then resetting the azimuth angle to zero and increasing the detector angle in 10 degree increments, varying the azimuth angle at each increment until all of the detector angles had been evaluated; and finallly, resetting the azimuth and detector angles to zero degrees and increasing the source angle in 10 degree increments while varying both azimuth and detector angles. The data sets that were taken are shown in Table 2.

Table 2

DAS Data Sets

DAS Data Set
XX-XX-30
XX-XX-40
XX-XX-50
XX-XX-60
XX-XX-70
XX-XX-80
XX-XX-90

The diffuse reflectance of the concrete sample's surface was measured on a Beckman DK-2A Spectrophotometer (appendix C).

Polarization error was checked by mounting a polarizing filter in front of the detector and rotating it. The projected field of view was then varied by moving the sample and the panels beneath the nadir and allowing all of each surface to be measured. Measurements, with and without the filter, were made at different DAS positions. The detector was also used to check the polarization properties of the incident flux from the source.

At the conclusion of the experiment, a mold of the concrete surface was made using a commercially available product. The mold, a rubber replicate of the surface texture, was measured on a profileometer at the Calspan Corporation in Buffalo, New York (appendix F).

RESULTS

The major problem encountered during this experiment was detector repeatability. To solve the repeatability problem it was necessary to make many of the detector modifications described earlier. Preliminary measurements taken at various DAS positions indicated that reflectance from the concrete surface would vary from about 29% to 40%. Many of the measurements taken at adjacent positions on the arch might vary by only one-half percent, so it was decided that the detector needed to be able to repeat measurements at the same position to within a quarter of a percent. Repeated reflectance measurements made by varying only the positions of the panels or sample beneath the projected field of view, showed the modified detector to have a standrd deviation of 0.317 percent reflectance or better. Results from repeatability checks at several different DAS positions are shown in Table 3.

Table 3

Detector Repeatability Results

DAS Position	Sample Size	Standard Deviation (%R)
60-60-60	60	0.317
60-120-60	41	0.168
60-150-40	39	0.102
60-210-40	30	0.100

The variance shown in Table 3 was attributed to variance in the detector and very minor errors in positioning the panels or concrete sample beneath the nadir each time. The positioning error was felt to be negligible since later measurements showed reflectance measurements taken across the surface of each panel and the concrete to be very uniform.

Checks on repeatability after one or more of the angles had been changed showed the system to have a larger variance, which was expected. The increase in variance was attributed to inexact replication of the exact source, detector, or azimuth angle, or a combination of these. Results are shown in Table 4.

Table 4

Detector Repeatability Results After Angles Had Been Changed and Realigned

DAS Position	Sample Size	Standard Deviation (%R)
60-60-60	10	0.334
60-120-120	10	0.307
50-150-40	10	0.608
50-210-40	10	0.648

Data from the detector linearity experiment was entered into a computer where a regression analysis routine called Minitab was performed. The high R-squared value of 0.9989 (s = 0.008) indicated that the data fit a linear equation well. An analysis of variance was calculated to prove linearity; see appendix D.

Geometrical symmetry was verified by taking repeated measurements at two different (but symmetrical) DAS positions and then repeating the process at two more symmetrical positions. DAS positions 60-60-60 and 60-120-120 were compared as were positions 60-150-40 and 60-210-40. A measurement from each panel and the concrete sample was taken at each position and then the source or detector was moved and the process repeated at a different DAS position. Ten measurements were taken at each position, and then the mean reflectance and standard deviation at each position were calculated. The means from DAS positions 60-150-40 and 60-210-40 were compared ($\alpha = 0.05$), as were the means from DAS positions 60-60-60 and 60-120-120, and shown to have no statistically significant difference. This was taken as proof that geometrical symmetry existed; see appendix G.

The intent of this project was to establish a mathematical relationship between detector, azimuth, and source angles and the reflectance from a concrete surface. Considerable care had been taken during the experiment to make sure that other variables were not introduced. It was logical then to begin modeling reflectance as a function of only the detector, azimuth, and soure angles. One of the major differences between this project and an earlier one (Welch 1967), was the availability of computer capabilities to handle a range of data points. Most of the modeling involved, used a computer's power to manipulate several thousand numbers in thousands of combinations.

A reflectance value at each DAS position was calculated by substituting the measured voltages into the following formula:

$$Rc = 16 + \Delta R\ ((Vc-V16)/(V56-V16)) \qquad (11)$$

where Vc = multimeter voltage reading from the concrete sample

V16 = multimeter voltage reading from the 16% reflectance panel

V56 = multimeter voltage reading from the 56% reflectance panel.

$\Delta R = 56-16 = 40$ (for the panels used).

The first set of data taken, DAS XX-XX-50, was analyzed after entering into a computer each reflectance value and the corresponding detector, azimuth, and source angles at which they were measured. Since there were two independent variables (the detector and azimuth angles) in this data set, it was initially enlightening to compare reflectance to detector angle and reflectance to azimuth angle separately. A computer routine was used to plot reflectance versus detector angle and reflectance versus azimuth angle to see if any relationships existed. Both plots had shapes that indicated a second order polynomial fit. The data points were then entered into Minitab so that regression analysis could be performed. Because of the angular relationships involved, it was felt that a trigonometric representation

of each angle would be the simplest to model. Percent reflectance was regressed against first and second order trigonometric values of the angles.

The trigonometric values examined included sine, cosine, and tangent. Since two independent variables were involved, it was appropriate to regress against an additional term to take into account the interaction between the two angles. This term was calculated by multiplying the trigonometric values of the two angles together, i.e., $\sin\Phi\sin\psi$, $\cos\Phi\cos\psi$, and $\tan\Phi\tan\psi$. Many multiple regression routines were run using various combinations of terms in building the model; see Table 5. The only models

Table 5

Initial Selection of Trigonometric Terms in Model

Terms Included in Model	R-Squared Value
$\sin\psi$, $\sin\Phi$	.127
$\cos\psi$, $\cos\Phi$	.005
$\tan\psi$, $\tan\Phi$	.009
$\sin\psi$, $\sin\Phi$, $\sin\psi\sin\Phi$	.125
$\cos\psi$, $\cos\Phi$, $\cos\psi\cos\Phi$	.671
$\tan\psi$, $\tan\Phi$, $\tan\psi\tan\Phi$	.007
$\sin^2\psi$, $\sin\psi$, $\sin\Phi$	.124
$\cos^2\psi$, $\cos\psi$, $\cos\Phi$	.052
$\tan^2\psi$, $\tan\psi$, $\tan\Phi$	.009
$\sin^2\Phi$, $\sin\psi$, $\sin\Phi$	.126
$\cos^2\Phi$, $\cos\psi$, $\cos\Phi$	.177
$\tan^2\Phi$, $\tan\psi$, $\tan\Phi$	.055
$\sin^2\psi$ $\sin\psi$, $\sin\Phi$, $\sin\psi\sin\Phi$	.122
$\cos^2\psi$, $\cos\psi$, $\cos\Phi$, $\cos\psi\cos\Phi$	.669
$\tan^2\psi$, $\tan\psi$, $\tan\Phi$, $\tan\psi\tan\Phi$	.007
$\sin^2\Phi$, $\sin\psi$, $\sin\Phi$, $\sin\psi\sin\Phi$	.125
$\cos^2\Phi$, $\cos\psi$, $\cos\Phi$, $\cos\psi\cos\Phi$	.796
$\tan^2\Phi$, $\tan\psi$, $\tan\Phi$, $\tan\psi\tan\Phi$	.053
$\sin^2\psi$ $\sin^2\Phi$, $\sin\psi$, $\sin\Phi$, $\sin\Phi\sin\psi$	.122
$\cos^2\psi$ $\cos^2\Phi$, $\cos\psi$, $\cos\Phi$, $\cos\Phi\cos\psi$	.796
$\tan^2\psi$ $\tan^2\Phi$, $\tan\psi$, $\tan\Phi$, $\tan\Phi\tan\psi$	.053

that approached a good fit were those that included cosine terms.

Upon examination of the regression results, the model best relating reflectance to azimuth angle and detector angle was selected; it took the following form:

$$R = f(\cos\Phi,\ \cos\psi,\ \cos\psi\cos\Phi,\ \cos^2\Phi) \qquad (12)$$

Each data set (with a constant source angle, θ, of 30, 40, 60, 70, 80, or 90 degrees) was then regressed through the same combination of cosine terms as the DAS XX-XX-50 data. The model selected gave the best fit (for all of the data sets) in relation to other possible models made with different combinations of terms, as illustrated in Table 6.

Table 6

Results of Fitting Data Sets to Model
Best Representing Data Set DAS XX-XX-50

DAS Data Set	R-Squared Value
XX-XX-30	0.880
XX-XX-40	0.875
XX-XX-50	0.796
XX-XX-60	0.800
XX-XX-70	0.678
XX-XX-80	0.523
XX-XX-90	0.802

An examination of Table 6 shows that the R-squared values tend to decrease as the source angle increases. This is at least

partially explained by the increasing error in azimuth angle as the source angle increased from 30 degrees to 90 degrees, and is described later in this section. Note that the R-squared value of the source angle at 90 degrees was comparable to that at a source angle of 50 or 60 degrees; it did not drop off as predicted. This was explained by the fact that, when the source angle was at 90 degrees, there was no effective azimuth angle between source and detector. The data, therefore, was not forced to fit the model as in the preceeding cases.

The next step in building the model was to create a master data file containing all of the specular reflectance data measurements and the value of their respective independent variables, θ, Φ, and ψ. Since three independent variables were now being considered, it was possible to have four different forms of interaction: between Φ and ψ as before, between θ and Φ, between θ and ψ, and between θ, Φ, and ψ. Trigonometric representations of the angles were again used with reflectance being regressed against first and second order cosine terms and first order interaction terms. A stepwise regression routine was used to regress reflectance against the ten predictors. The model selected to predict specular reflectance was a function of ($\cos\theta\cos\Phi\cos\psi$, $\cos^2\theta$, $\cos^2\Phi$, $\cos\theta$, and $\cos\Phi$):

$$R = 32.14 - 4.25(\cos\theta\cos\Phi\cos\psi) + 1.88\cos^2\Phi + 3.96\cos^2\theta + 0.598\cos\Phi - 2.07\cos\theta. \quad (13)$$

where θ = source angle

Φ = detector angle

ψ = azimuth angle

Some typical plots of this function are shown in appendix H. This model, computed from a sample size of 1,527 measurements, had an R-squared value of 0.78 and a standard error of 0.645. The reflectance measurements made ranged from 30.07 to 41.61 percent. An examination of standardized residuals plotted against reflectance showed no apparent trend. The presence of a pattern or shape would have indicated that there might be a missing term. The random pattern present did not suggest the need for an additional term in the model. Although this model may seem complex since it contains five terms with variables, remember that there are three independent variables alone, and the model must account for the geometrical effects described earlier. Using this model, it was possible to predict the specular reflectance to within plus or minus 1.3% (2 σ) if the DAS angular relationship was known.

The diffuse reflectance of the concrete surface, measured on a Beckman DK-2A Spectrophotometer, was 34%; see appendix C.

To make an accurate model which would work outdoors, it was necessary to weight and combine the diffuse and specular reflectance values. This weighting would determine what proportion of the reflectance value was from specular sunlight and

what was from diffuse skylight. Hulburt's sunlight to skylight ratios were used. As shown in the introduction, these ratios were dependent on sky condition and went from a high of 7:1 to a low of 1:1. The weighting factors selected were also recommended by Peich and Walker, and Lillesand. On a clear day the model would be of the form:

$$R = 7/8 \text{ (specular model value)} + 1/8 \text{ (diffuse value)}. \quad (14)$$

On a hazy day the model would be:

$$R = 3/4 \text{ (specular model value)} + 1/4 \text{ (diffuse value)}. \quad (15)$$

On a light overcast day the model would be:

$$R = 1/2 \text{ (specular model value)} + 1/2 \text{ (diffuse value)}. \quad (16)$$

An observor would be required to select the appropriate model on the basis of his estimation of sky conditions, and this would not be difficult on a clear-sky day. (High altitude imaging on an overcast day makes the selection of a model academic.)

To test the model, outdoor measurements needed to be made. The outdoor measurements were taken on a clear sunny day during the winter. The arches, detector, cart, and associated equipment were set up on the athletic field track at the Rochester

Institute of Technology. The apparatus was assembled far enough away from any buildings, trees, or other obstacles that they would not provide a source of background illumination (Schott, 1982). Measurements were taken on the hour at detector positions of 30, 60, 110, and 130 degrees. As the day progressed, the sun's movement across the sky provided variations in sun (source) angle and azimuth angle. Because of the time of year, the maximum sun angle during the day was 45 degrees. Measurements were taken only during the time of day when the sun angle would be greater than 30 degrees.

A total of nineteen separate DAS positions were evaluated, with three replicate measurements made at each DAS position. Since the measurements were made on a clear day, the first model was selected.

Sun and azimuth angles were calculated from a program developed for a pocket calculator. Several program inputs were needed, including Greenwich Hour Angle, Local Hour Angle, Solar Declination Angle, and the longitude and latitude of the RIT campus. The Solar Declination Angles and Greenwich Hour Angles for the times of measurement were obtained from a Nautical Almanac. Latitude and Longitude were determined from an air navigational chart. Local Hour Angles (LHA) were calculated from the Greenwich Hour Angles and the longitude. Values for the LHA, Solar Declination Angle, and latitude were then input into a program which yielded the sun and azimuth angles for the

time of measurement. The equations and techniques used were verified by Dr. Savedoff, an astronomy professor at the University of Rochester.

Table 7 below lists the predicted measurements and the actual outdoor measurements by DAS position. As the table below shows, the outdoor reflectance measurements agreed to within plus or minus one percent reflectance in almost every case.

Table 7

Predicted Reflectance Measurements From Model Versus Actual *

DAS Position	Specular Prediction	Predicted Total R	Actual Reflectance	Error
60-136-36	35.1	35.0	33.8	+1.2
110-136-36	32.2	32.4	32.2	+0.2
130-136-36	31.9	32.2	32.0	+0.2
30-174-46	37.1	36.7	37.0	-0.3
60-174-46	34.9	34.8	33.9	+0.9
110-174-46	31.6	31.9	32.2	-0.3
130-174-46	31.1	31.5	30.2	+1.3
30-196-45	37.1	36.7	37.2	-0.5
60-196-45	34.9	34.8	33.9	+0.9
110-196-45	31.7	32.0	32.3	-0.3
130-196-45	31.2	31.6	32.2	-0.6
30-215-40	37.1	36.7	36.9	-0.2
60-215-40	35.0	34.9	34.1	+0.8
110-215-40	32.0	32.3	32.5	-0.2
130-215-40	31.6	31.9	32.9	-1.0
30-231-32	37.1	36.7	37.4	-0.7
60-231-32	35.1	35.0	33.7	+1.3
110-231-32	32.5	32.7	33.1	-0.4
130-231-32	32.2	32.4	32.9	-0.5

Predicted Range of Reflectance	31.5 - 36.7
Actual Range of Reflectance	30.2 - 37.4
Standard Error	0.739

* All numerical values are percent reflectance

The measurements validate the model by demonstrating that the predicted values are realistic.

The question as to whether or not this is a precise or even reasonable model needs to be addressed. Certainly the coefficients are at best approximations and the author would make no claim to nonvariable values here. The crux of the matter is the appropriateness of the trigonometric terms included in the model. It is known that all three angles θ, Φ, and ψ, are independent of each other. Egbert and Ulaby's (1972) work demonstrated that the model needs to contain at least one term for each of the variables (angles). From plots of reflectance versus Φ and reflectance versus ψ, it is apparent that reflectance changes as the angles change. There should not be a problem accepting, as reasonable, a model containing one or more than one of these terms. It is also reasonable to expect interaction effects between the three variables. Is it reasonable though to expect second order trigonometric terms in the model, and is it reasonable to consider all of the angles in terms of cosine values? For the universal model perhaps not, but for this particular model first and second order cosine terms provided the best fit to the data, hence they were included.

Various sources of error, which may have contributed to the data on which the model was based, were investigated, including panel positioning error, polarization error, errors

in reading the multimeter, and imprecise azimuth poisitioning.

Panel positioning error, as mentioned earlier, was found to be negligible.

Polarization error was also found to be negligible. The source was checked and found to be a random polarizer, so it did not contribute. No polarization from the concrete or the reflectance panels was detected, even at the extreme incident and viewing angles of DAS 30-0-150.

Errors in reading the last digit displayed on the multimeter did contribute error in the data, and consequently, the reflectance values. The last digit displayed tended to fluctuate, causing the reading to vary by plus or minus 0.001 units. For example, a value of 1.136 might read 1.135, 1.136, or 1.137 depending on when it was taken. This error was taken into account in calculating the standard deviation of the repeatability checks on the detector.

While the detector and source angles could be set precisely, the azimuth angle involved an inherent error because of the constant offset of the detector or source from the arch. Because of the mounting arrangements on the arches, the center of the apertures of both the detector and source were offset from the center of the arch. Although the offset was constant, the error in azimuth angle increased as the source or detector position was increased toward ninety degrees. This was due to the fact that the azimuth angle actually existing was formed by the arc from

the projected position of the detector to the projected position of the source, and not the arc from the detector's arch to the source's arch. At a source angle of thirty degrees, the azimuth offset error was 2.15 degrees; at a source angle of eighty degrees the azimuth offset error had increased to 10.6 degrees, a four fold increase. This error could have been corrected out but was not since the azimuth angle was the least significant of the three angles involved. Egbert and Ulaby demonstrated that the azimuth angle is the least significant angle of the three involved. This fact was confirmed from a close examination of the reflectance model which showed only a single first order consideration of the angle's cosine value.

The azimuth error may have contributed to the decreasing R-squared values shown in Table 6. The contribution was significant in that case because two of the four terms in the initial model contained azimuth terms.

CONCLUSION

This thesis was an initial step towards quantitatively accounting for the sun-object-image angular relationship when determining reflectance values. The results from this project have shown that it is possible, at least for this particular concrete sample, to predict the percent reflectance very accurately (within one percent) if the sun-object-image angular relationship is known.

The main advantage to using a reflectance value which has been adjusted for the sun-object-image angular relationship rather than a mean reflectance value is that it allows someone using the Scene Color Standard technique to determine a more accurate reflectance value for a target. This might permit an air photo interpreter analyzing an image by spectral pattern recognition techniques to make better decisions. Taking into account the sun-object-image angular relationship present when an image was made allows a more accurate value for concrete reflectance to be determined. Using a better value for concrete reflectance in the regression routine results in a more accurate exposure/reflectance linear equation. A better linear equation yields a better value for the target's reflectance when its exposure value is substituted into the equation.

For example, assume that a target was imaged on a piece of

film that also contained images of concrete and asphalt roadways. The densities of both roadway images and the unknown target could be measured and converted into exposure units. In this example assume that the exposure values for the concrete, target, and asphalt were 187, 135, and 110, respectively. Using Piech and Walker's average reflectance values for asphalt and concrete of 18 and 30%, a regression routine could be run, yielding an equation for the line connecting the asphalt and concrete points,

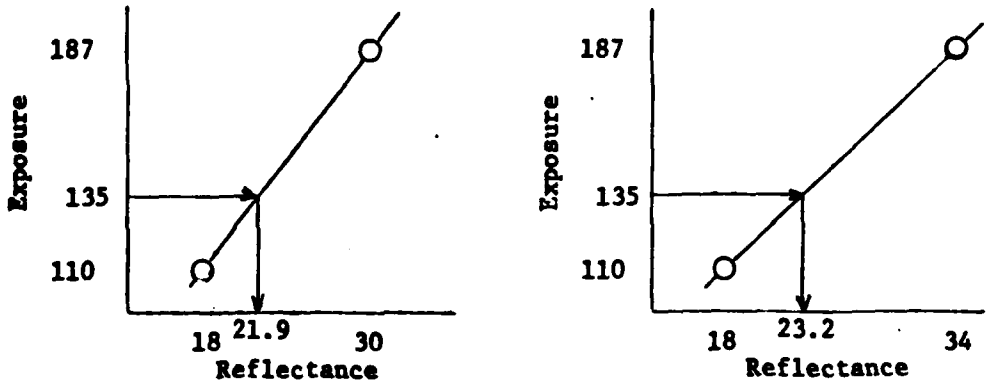

A B

Uncorrected (A) Versus Corrected (B) Plots of $E = \alpha R + \beta$

Figure 22

as plotted in figure 22 A. Substituting the target's 135 exposure value into the equation yields a reflectance value of 21.9%. Now assume that after considering the sun-object-image

angular relationship at the time the image was recorded, it was determined that the reflectance value for concrete was 34% rather than 30%. Regressing this new value yields a different linear equation; and when the target's exposure value of 135 is substituted into the linear equation, its expected reflectance value turns out to be 23.2%; see figure 22 B. This is an improvement in accuracy of 1.3 percent reflectance.

The model derived in this project applies to just this particular surface. Good scientific procedure dictates repeating the experiment several more times before any conclusive statements are made. Several variations of this experiment should also be made, including checking the effects of different wavelengths and different surface textures. Comparisons should be made between all the models generated, looking for similarities and differences.

Although concrete samples with different surface textures were not evaluated, several generalizations about surface texture and geometric effects upon reflectance can be inferred. A smoother surface would have less differential shading but more specular reflection effects. A smoother surface would probably show a wider absolute range in reflectance values as the source and detector were varied throughout the hemisphere above the surface. Conversely, a rougher surface would probably have a narrower range of reflectance values since differential shading would be more of a factor, and specular reflection less.

On a smooth surface specular reflection (viewed from certain angles) and diminished differential shading effects would both act to drive up the absolute reflectance value. On a rough surface more of the area would be covered by shadows (a smaller surface area illuminated) because of differential shading effects, and specular reflection would not be as big a factor. Both effects would act together to diminish the absolute reflectance value.

It might prove possible for a future researcher to derive a more universal concrete reflectance model. If so, adaptations might be made which would make the model applicable to asphalt and other paved surfaces. The model derived in this thesis project is an important first step because it shows that the reflectance from a surface can be modeled with greater accuracy when the sun-object-image angular relationship is included.

BILIOGRAPHY

Biegel, Joesph D. Conversations with the author.

Billingsley, Frederic C. "Image-Data-Processing for Earth Resources - An Overview." Journal of Applied Photographic Engineering, 8 (February 1982): 2-14.

Breece, H. T., and Holmes, R. A. "Bidirectional Scattering Characteristics of Healthy Green Soybean and Corn Leaves in Vivo. "Applied Optics, 10 (January 1971): 119-127.

Coulson, Kinsell L. "Effects of Reflection Properties of Natural Sciences in Aerial Reconnaissance." Applied Optics, 5 (June 1966): 905-917.

Coulson, K. L., and Reynolds, David W. "The Spectral Reflectance of Natural Surfaces." Journal of Applied Meteorology, 10 (December 1971): 1285-1294.

Craig, Charles D. and Loury, William P. "Reflections on the Urban Albedo." Handout, p. 159-164.

Dave, J. V., "Effect of Atmospheric Conditions on Remote Sensing of a Surface Nonhomogeneity." Photogrammetric Engineering and Remote Sensing, 46 (September 1980): 1173-1180.

Draper, Norman R., and Smith, Harry. Applied Regression Analysis. New York, New York: John Wiley & Sons, Inc., 1966.

Duggin, M. J., "Rapid Communications." Applied Optics, 16 (March 1972): 521-523.

Egbert, Dwight D., and Ulaby, Fawwaz T. "Effects of Angles on Reflectivity." Photogrammetric Engineering, 38 (June 1972), 556-564.

Fowler, B.; Reed, E. I.; and Blamont, J. E. "Bidirectional Reflectance of the Moonlit Earth." Applied Optics, 10 (December 1971): 2657-2660.

Gallagher, Tim W. Conversations with the author.

Hunt, Graham R., and Ross, Howard P. "A Bidirectional Reflectance Accessory for Spectroscopic Measurements." Applied Optics, 6 (October 1967): 1687-1690.

Irons, James R., and Labovitz, Mark L. "A Data Analytic Approach to Look-Angle Radiance Adjustment." Journal of Applied Photographic Engineering, 8 (June 1982): 128-137.

Jackson, R. D.; Pinter, P. J. Jr.; and Reginto, R. J. "Wheat Reflectance: Interactions Between Crop Configuration, Sun Elevation, and Azimuth Angle." Applied Optics, 18 (November 1979): 3730-3732.

Kodak Publication B-3, Kodak Filters for Scientific and Technical Uses, 1978.

Lillesand, Thomas M., and Kiefer, Ralph W. Remote Sensing and Image Interpretation. New York: John Wiley & Sons, 1979.

Longshaw, T. G. "Field Spectroscopy for Multispectral Remote Sensing: An Analytical Approach." Applied Optics, 13 (June 1974): 1487-1493.

McDowell, D. Q. "Spectral Distribution of Skylight Energy for Two Haze Conditions." Photogrammetric Engineering, 40 (May 1974): 569-571.

McDowell, D. Q., and Specht, M. R. "Determination of Spectral Reflectance Using Aerial Photographs." Photogrammetric Engineering, 40 (May 1974): 559-568.

Palmer, James M., "Field Standards of Reflectance." Photogrammetric Engineering and Remote Sensing, 48 (October 1982): 1623-1625.

Piech, Kenneth R., and Walker, J. E. "Interpretation of Soils." Photogrammetric Engineering, 40 (January 1974): 87-94.

Piech, Kenneth R., and Schott, John R. "The Blue-to-Green Reflectance Ratios and Lake Water Quality." Photogrammetric Engineering and Remote Sensing, 44 (October 1978): 1303-1310.

Piech, Kenneth R., and Walker, J. E. "Aerial Color Analysis of Water Quality." Journal of Surveying and Mapping Division, American Society of Civil Engineers, 97 (1971): 185-197.

Piech, Kenneth R., and Walker, J. E. "Thematic Mapping of Flooded Acreage." Photogrammetric Engineering, 38 (Nov 1972): 1081-1096.

Reeves, R. G., ed. Manual of Remote Sensing Vol. I. Falls Church, Virginia: American Society of Photogrammetry, 1975.

Rubin, Jacob C. Conversations with the author.

Ryan, Thomas A. Jr.; Ryan, Barbara F.; and Janier, Brian L. Minitab Reference Manual. Boston, Massachusetts: Duxbury Press, 1981.

Salomonson, Vincent V., and Marlatt, William E. "Airborne Measurements of Reflected Solar Radiation." Remote Sensing of Environment, 2 (1971): 1-8.

Schott, John R. "Exposure Reaching an Airborne Camera System." Lecture Notes PPHS 752, March 1982.

_____. "Temperature Measurement of Cooling Water Discharged from Power Plants." Photogrammetric Engineering and Remote Sensing, 45 (June 1979): 753-761.

_____. Conversations with the author.

Slater, Phillip N. Remote Sensing: Optics and Optical Systems. Reading, Massachusetts: Addison-Wesley Publishing Company, 1980.

Smith, J. A., and Oliver, R. E. "Effects of Changing Canopy Directional Reflectance on Feature Selection." Applied Optics, 13 (July 1974): 1599-1604.

Steiner, Dieter, and Haefner, Harold. "Tone Distortion for Automated Interpretation." Photogrammetric Engineering, 31 (March 1965): 269-280.

Swain, Philip H., and Davis, Shirley M., eds. Remote Sensing: The Quantitative Approach. New York, New York: McGraw-Hill Inc, 1978.

Walker, Patrick M., and Trexler, Dennis T. "Low Sun Angle Photography." Photogrammetric Engineering and Remote Sensing, 43 (April 1977): 493-505.

Welch, Guy F. "Variations in the Spectral Radiometric Function, Measured in the Field, of Five Different Types of Terrain as a Function of Atmospheric Conditions, Solar Altitude, and Viewing Position." MS Thesis, Rochester Institute of Technology, 1967.

Appendix A

Exposure Reaching an Airborne Camera System (Schott, 1982)

Let I represent the radiant intensity from the sun [W/Sr].

Then the irradiance on the earth's surface from the sun will be

$$E_{sun} = I\ T/d^2\ [W/m^2]$$

Where T is the atmospheric transmission from deep space to the earth's surface and d is the distance from the earth to the sun.

The radiation passing through the atmosphere will be scattered proportional to e^{-bx} where b is the scattering coefficient [1/meters] and x is the path length through the atmosphere.

The total scattered radiation will be a function of the source strength I and the amount of scatter e^{-bx}

Therefore

$$E_{sky} = f(I, e^{-bx})\ [W/m^2]$$

represents the diffuse irradiance on the surface from sunlight scattered by the atmosphere.

The total irradiance incident on the earth's surface can therefore be expressed as

$$E_I = E_{sun} + E_{sky} = IT/d^2 + f(I, e^{-bx})\ [W/m^2]$$

The radiant exitance reflected from the earth's surface can be expressed as

$$W = E_I r\ [W/m^2]$$

where r is the reflectance of the object observed

The radiance from the reflecting surface can be expressed as

$$L = \frac{dW}{d\omega \cos\theta}\ [W/m^2 sr]$$

Where ω is the element of solid angle and θ is the angle from the normal to the surface.

Then

$$dW = L\ d\omega \cos\theta$$

And

$$W = \int L\ d\omega \cos\theta$$

If the surface is lambertion (i.e., of perfectly diffuse reflection) then the radiance is independent of θ and

$$W = L \int d\omega \cos\theta = L\pi$$

or

$$L = \frac{W}{\pi} \ [W/m^2 sr]$$

substituting in equation 4 above yields

$$L = \frac{E_{sun}\, r}{\pi} + \frac{E_{sky}\, r}{\pi}$$

Expressing the reflected target strength in radiance is convenient because in the case of a perfect atmosphere the radiance reaching an airborne sensor at any altitude is the same as the radiance at the source.
Thus the radiance reaching the airborne platform at altitude h is

$$L_h = \tau L + B \ [W/m^2 sr]$$

Where τ is the atmospheric transmission from the target to the aircraft.
And B is the radiance due to the light scattered upward by the air column beneath the sensor.
The irradiance on the film in a camera is related to the radiance reaching the camera by the G number
i.e., $E = L/G \ [W/m^2]$
where $G = f(A, \tau')$

A is the f # of the lens, τ' is the lens transmission

Thus the irradiance on the film in an aerial camera can be expressed as

$$E_f = L_h/G + b \ [W/m^2]$$

$$= \frac{E_{sun}\, r\tau}{\pi G} + \frac{E_{sky}\, r\tau}{\pi G} + \frac{B}{G} + b$$

where b is camera flare.
The exposure H on the film is given by

$$H = E_f \cdot t \ [W \cdot s/m^2]$$

$$= \frac{E_{sun}\, r\tau t}{\pi G} + \frac{E_{sky}\, \tau r t}{\pi G} + \frac{Bt}{G} + bt$$

Simplfying this expression

$$H = \gamma r + \alpha' r + \beta$$

Letting exposure H be expressed as E after Lillesand

$$E = H = \gamma r + \alpha' r + \beta$$
$$= \alpha r + \beta$$

where γ represents the sunlight component and α' represents the skylight component.

In terms of Lillesand's analysis

$$E = k_3 R + K_4$$

or $$R = \frac{E - \beta}{\alpha} = \frac{10^{Z(D)} - \beta}{\alpha}$$

Appendix B

Uniformity of the Source's Projected Illumination Spot

The uniformity of the collimated source's illumination across the 16% panel was checked. A half inch diameter projected spot size was measured by installing a bifurcating mirror with a smaller aperture in the detector. Measurements were taken in both the x and y directions. Because of limitations in the detector's movement, x and y axis directions had to be taken from different DAS (Detector-Azimuth-Source) positions. X and y axis measurements were taken at DAS positions 60-0-110 and 60-90-110, respectively. Figure 23 shows the positions within the source's projected spot size where the measurements were recorded.

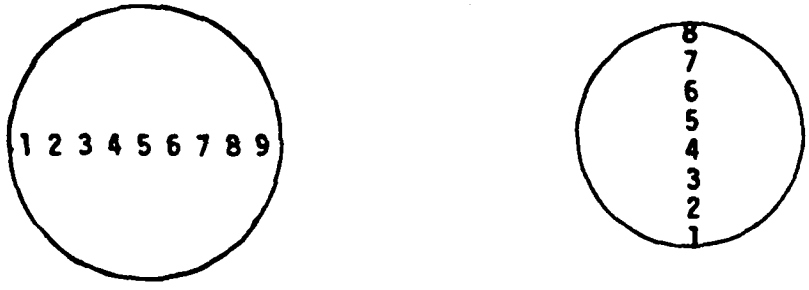

Measurement Positions Within Projected Spot Size

Figure 23

Measurements in the x direction were taken at 0.6 inch intervals while those in the y direction were taken at 0.7 inch intervals. The uniformity of the measured voltages is shown in Table 8.

Table 8

Data From Source Illumination Uniformity Check

X Axis		Y Axis	
Position	Voltage	Position	Voltage
1	.958	1	.942
2	.961	2	.945
3	.963	3	.950
4	.966	4	.950
5	.966	5	.950
6	.966	6	.947
7	.966	7	.945
8	.963	8	.942
9	.959		
$\bar{x}$	0.9631	$\bar{x}$	0.946
n	9	n	8
s	0.0032	s	0.0034
$s/\bar{x}$	0.0033	$s/\bar{x}$	0.0036

Where $\bar{x}$ and s are the mean and standard deviation of the sample population. The low $s/\bar{x}$ values in the x and y directions meant that illumination was uniform over the projected spot.

Appendix C

Beckman DK-2A Diffuse Reflectance Data

The reflectance from each of the six panels was measured on a Beckman DK-2A Spectrophotometer. The spectrophotometer had the capability to measure either total (diffuse plus specular) or diffuse reflectance. Both total and diffuse reflectance were measured and compared. Subtracting the diffuse value from the total value yielded the specular value. As table 9 shows, the specular values were essentially zero. Almost all of the reflectance from the panels was diffuse, which meant the panels were near-Lambertian.

A simple experiment was run to verify that the panels were near-Lambertian. The 16% reflectance panel was placed beneath the zenith of the arches and illuminated with diffuse lighting. The detector was placed at 19 randomly selected DAS positions, and the voltage measured at each position was recorded. A perfect Lambertian reflector would have had identical readings regardless of the azimuth or detector angle. The measured volt ages were then averaged. This average was converted to a 16.4 percent reflectance value (standard deviation of 0.83 percent reflectance). These results verified that the panel was indeed close to being a Lambertian reflector.

The reflectance from the concrete sample was measured on the Beckman DK-2A Spectrophotometer on two different occasions. Both times it had a diffuse reflectance value of 34.0%. Measurements

were also taken with the Spectra Spotmeter from sixteen different

Table 9

Beckman Spectrophotometer Data Results

Reflectance Panel	% Reflectance (Total)	% Reflectance (Diffuse)	% Reflectance (Specular)
16	15.9	15.9	0.0
26	25.9	25.5	0.4
30	29.9	29.6	0.3
56	56.2	56.2	0.0
73	72.5	72.5	0.0
93	93.2	93.0	0.2

positions. Diffuse lighting was simulated by placing two sheets between the overhead room lamps and the arches. The average reflectance value from the sixteen positions was 34.08%. A diffuse reflectance value of 34.0% was used to construct the model.

Appendix D

Detector Linearity Check

To demonstrate that the detector had a linear response, five measurements were taken from five panels of different (but known) reflectance. The measurement procedure consisted of moving the five panels, in succession, under the zenith of the arches and recording the voltages displayed on the multimeter. The process was repeated five different times to check on repeatability. Data from the measurements is shown in table 10.

Table 10

Data From Detector Linearity Check

Percent Reflectance	Measured Voltage	Percent Reflectance	Measured Voltage
16	1.068	30	1.231
16	1.066	30	1.231
16	1.064	56	1.546
16	1.061	56	1.542
16	1.060	56	1.541
26	1.192	56	1.539
26	1.188	56	1.539
26	1.187	73	1.719
26	1.184	73	1.717
26	1.184	73	1.715
30	1.239	73	1.715
30	1.236	73	1.713
30	1.233		

When the measured voltage was plotted against percent reflectance a linear relationship was apparent, see figure 24.

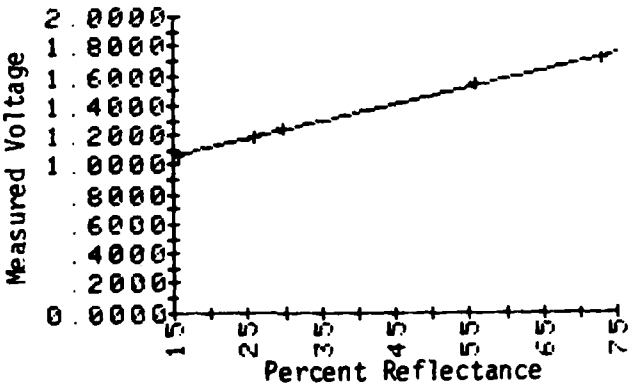

Plot of Measured Voltage Versus Percent Reflectance

Figure 24

The data points were then enterd into a computer which performed a regression analyis. The calculated R-squared value was .9989, with a standard deviation of 0.711 percent reflectance. An analysis of variance, including lack of fit, was then calculated. As table 11 shows, almost all of the variance was accounted for by the regression, and very little by the residual. The results of the f test however, indicated a lack of fit to the model. After consulting Draper and Smith's text on regression analysis, a plot was made of the standardized residuals versus the order (by time) in which the measurements were made. This plot indicated a trend in the data collection, see figure 25. The trend, which accounted for the lack of fit, was traced back to a drift, over time, in the detector. The detector's response was linear, but

the drift needed to be eliminated.

Mr. Tim Gallagher, the Institute's expert on detector repair, investigated and concluded that nothing could be done to

Table 11

Analysis of Variance Table

Source	Sum of Squares	Degrees Freedom	MS	f
Regression	1.461137	1	1.461137	153,159
Residual	0.000884	23		
Lack of fit	0.000693	3	0.0002313	24.24
Pure error	0.000191	20	0.0000095	
Total	1.462014	24		

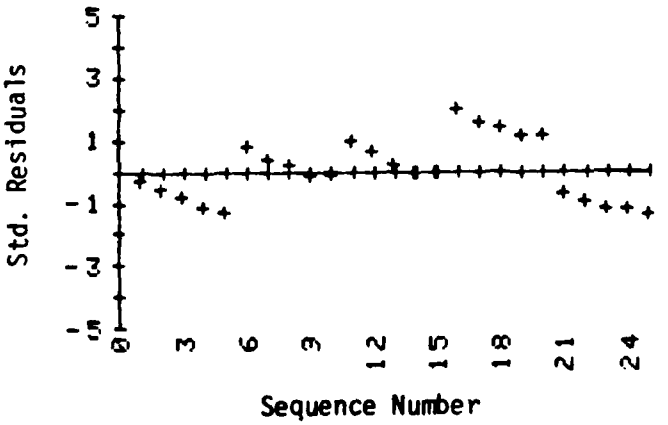

Plot of Standardized Residuals Versus Order of Measurements

Figure 25

AD-A132 511 CERTIFICATE OF APPROVAL(U) AIR FORCE INST OF TECH 2/2
WRIGHT-PATTERSON AFB OH G C GROGAN JUN 83
AFIT/CI/NR-83-18T

UNCLASSIFIED F/G 20/6 NL

END
DATE FILMED
DTIC

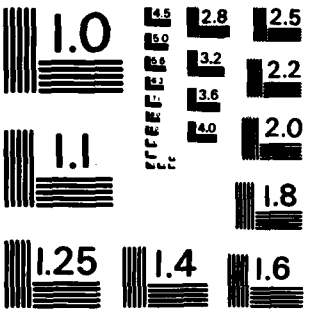

prevent the drift. During consultations with Dr. Schott and Mr. Gallagher, it was decided that acceptable results could be achieved if the measurements at each DAS position were taken within a short time span (30 seconds). This technique was valid since the reflectance panel measurements would allow a new linear relationship to be established at each DAS position.

Appendix E

Panel Uniformity Measurements

Nine separate measurements were taken across the surface of each panel and the concrete sample in order to check the uniformity of both the surface's texture and color. The panels and concrete sample were placed, one at a time, under the zenith of the arches so that the projected spots from the detector and source were just within the border of the panel (or sample). A voltage measurement was taken and the cart was pushed approximately 0.3 inches before another measurement was taken. The cart was pushed in 0.3 inch increments until the projected spots had traveled across the surface and were just within the opposite border. Measurements were taken across the surface, in the numerical order illustrated in figure 26.

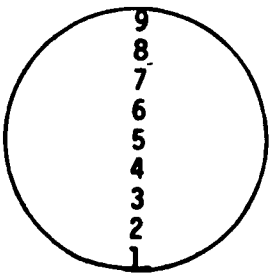

Position of Measurements Across Sample and Panels

Figure 26

The actual measurements are shown in Table 12. The symbols $\bar{x}$ and s denote the mean and standard deviation of the sample population. The low values of $s/\bar{x}$ indicated surface uniformity. As expected, both reflectance panels had lower $s/\bar{x}$ values than the concrete sample indicating greater uniformity of reflectance across the panels.

Table 12

Surface Uniformity Measurements

Position	Voltage Reading		
	16%	C1	56%
1	1.018	1.185	1.433
2	1.016	1.188	1.432
3	1.015	1.181	1.429
4	1.015	1.184	1.429
5	1.015	1.186	1.430
6	1.015	1.186	1.430
7	1.014	1.188	1.431
8	1.014	1.186	1.429
9	1.014	1.184	1.430
$\bar{x}$	1.0151	1.1853	1.4303
s	0.0013	0.0022	0.0014
$s/\bar{x}$	0.0013	0.0018	0.0010

Appendix F

Surface Roughness Measurement

The surface roughness of the concrete sample was measured with a surface profileometer at the Calspan Corporation in Buffalo, N.Y. A mold, one inch in diameter, of the center of the surface was prepared from "Rubbergel" material manufactured by Westwood Pharmaceuticals. The rubber surface of the mold was then analyzed on a Gould Surfalyzer. The mold was positioned under a delicate probe (similar to a turntable stylus) which translated the surface height variations into electrical signals that were recorded relative to the translation of the probe on the surface. The signals were recorded on a strip chart; see figure 27.

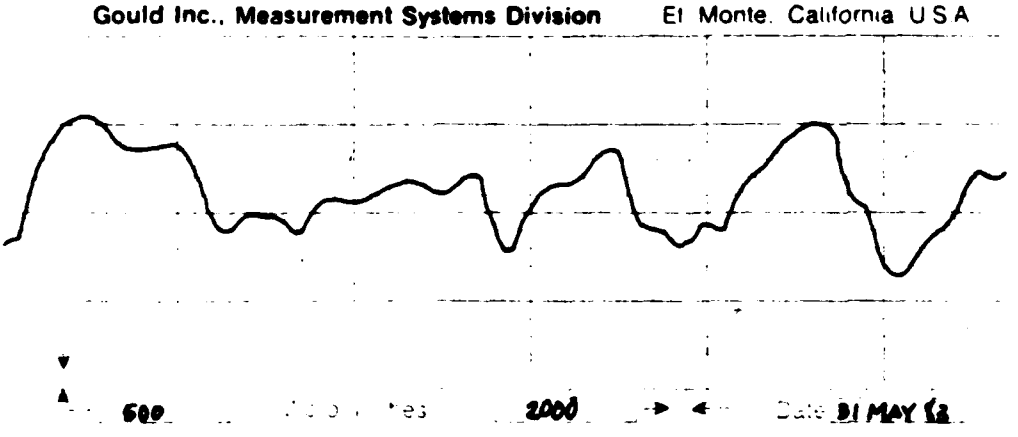

Portion of the Strip Chart Containing Surface Roughness Data

Figure 27

Analysis of the chart yielded a roughness average value of 0.001294 inches. This is the arithmetic average of the absolute values of the measured profile height deviations (taken every two thousandth of an inch) within the sampling length and measured from the graphical centerline.

Appendix G

DAS Symmetry Check

Geometrical symmetry nullified the requirement for measuring reflectance at symmetrical DAS positions. Symmetry was proven by statistically comparing reflectance measurements taken at DAS positions 60-60-60 and 60-120-120. DAS positions 50-150-50 and 50-210-50 were also compared. The null hypothesis was that there was no difference in the average of the ten reflectance measurements made at each position.

Null Hypothesis: $\mu_1 = \mu_2$

Assume that $\sigma_1 = \sigma_2$, but unknown. Test with T Distribution:

$$\text{Use} \quad t = \frac{\bar{x}_1 - \bar{x}_2}{S_p\sqrt{\frac{1}{n_1} + \frac{1}{n_2}}} \qquad S_p^2 = \frac{(n_1 - 1)s_1^2 + (n_2 - 1)s_2^2}{n_1 + n_2 - 2}$$

Number of degrees of freedom = $n_1 + n_2 - 2 = 10 + 10 - 2 = 18$
Critical Region ($\alpha = 0.05$ and 18 d.f.) $T > 1.734$ or $T < -1.734$

Consider DAS 60-60-60 Symmetry with DAS 60-120-120:

60-60-60: $\bar{x}_1 = 33.093$ $n_1 = 10$ $s_1^2 = 0.0371$
60-120-120: $\bar{x}_2 = 33.134$ $n_2 = 10$ $s_2^2 = 0.0313$

Solving on a computer yielded $t = -0.4957$.

Consider DAS 50-150-50 Symmetry with DAS 50-210-50:

50-150-50: $\bar{x}_1 = 34.693$ $n_1 = 10$ $s_1^2 = 0.1233$
50-210-50: $\bar{x}_2 = 34.542$ $n_2 = 10$ $s_2^2 = 0.1398$

Solving on a computer yielded $t = 0.9311$.

Conclusion: In both cases, the "t" value calculated does not exceed the critical value. Statistically, this means that we accept the null hypothesis since it can not be rejected. Therefore, the DAS positions are considered symmetrical.

Appendix H

Specular Reflectance Plots

This appendix contains representative plots of specular reflectance versus either detector, azimuth, or source angle. The specular reflectance model derived during this experiment was used to generate the curves. Actual data points (plotted as plus symbols) are shown on some of the graphs to illustrate how well the model fit the data.

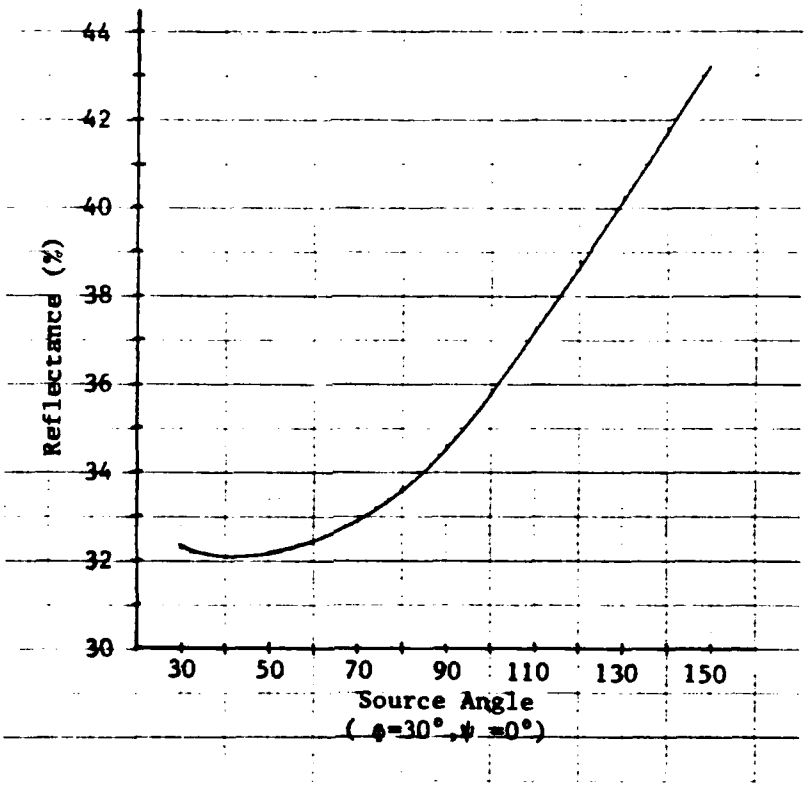

Plot of Specular Reflectance Versus Source Angle

Figure 28

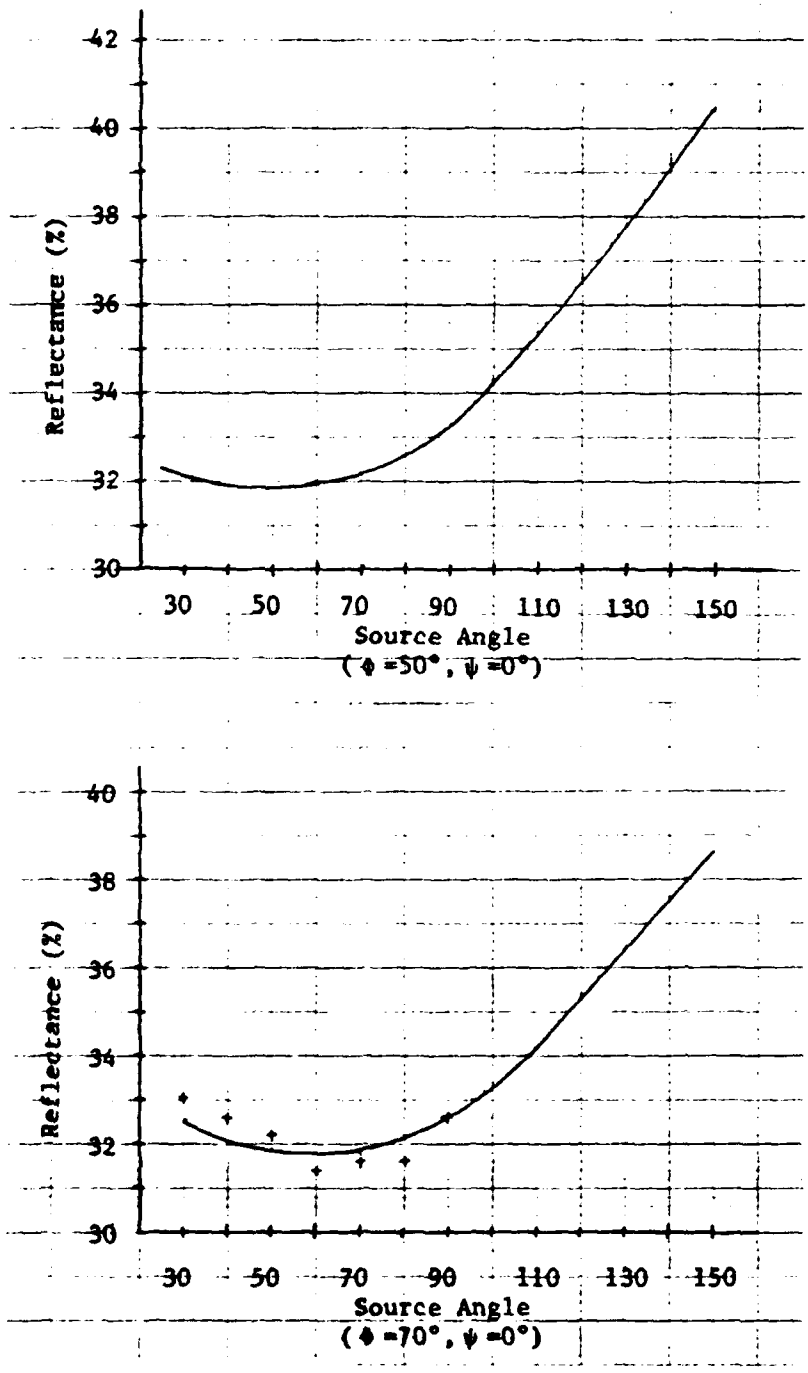

Plots of Specular Reflectance Versus Source Angle

Figure 29

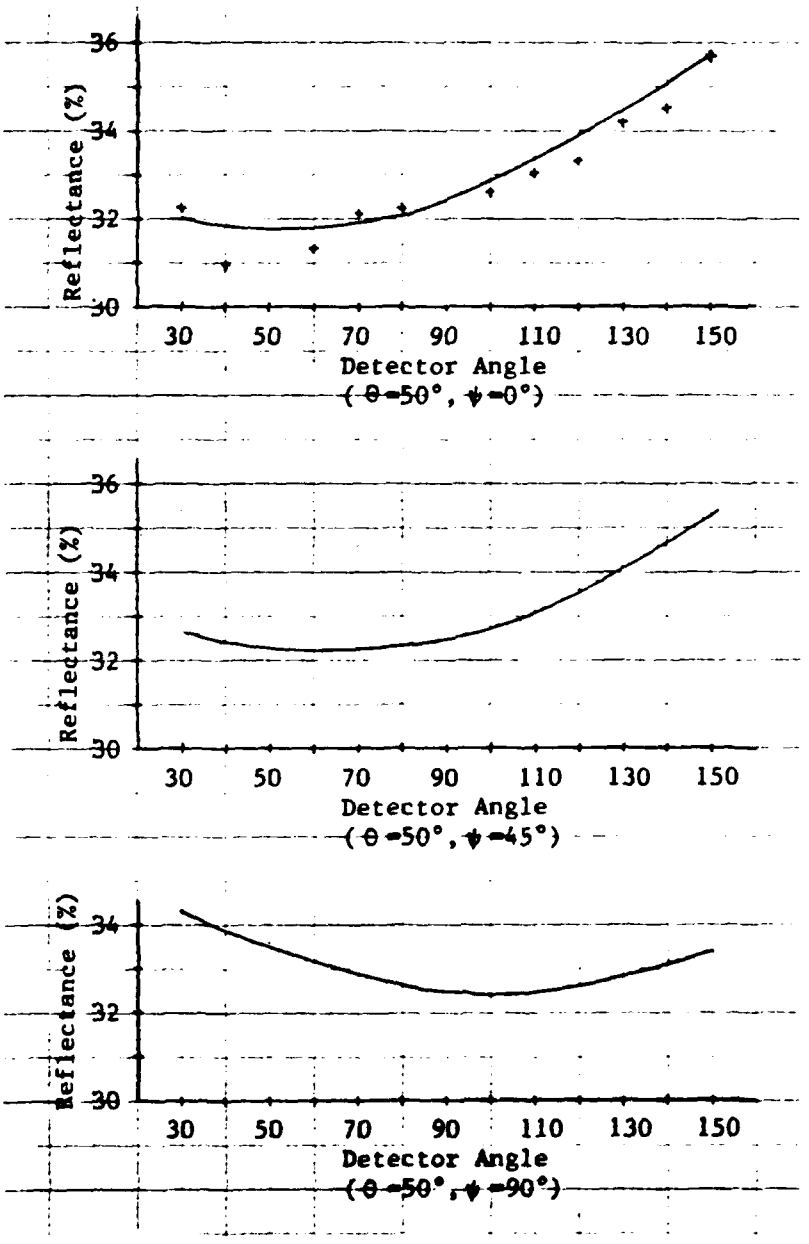

Plots of Specular Reflectance Versus Detector Angle

Figure 30

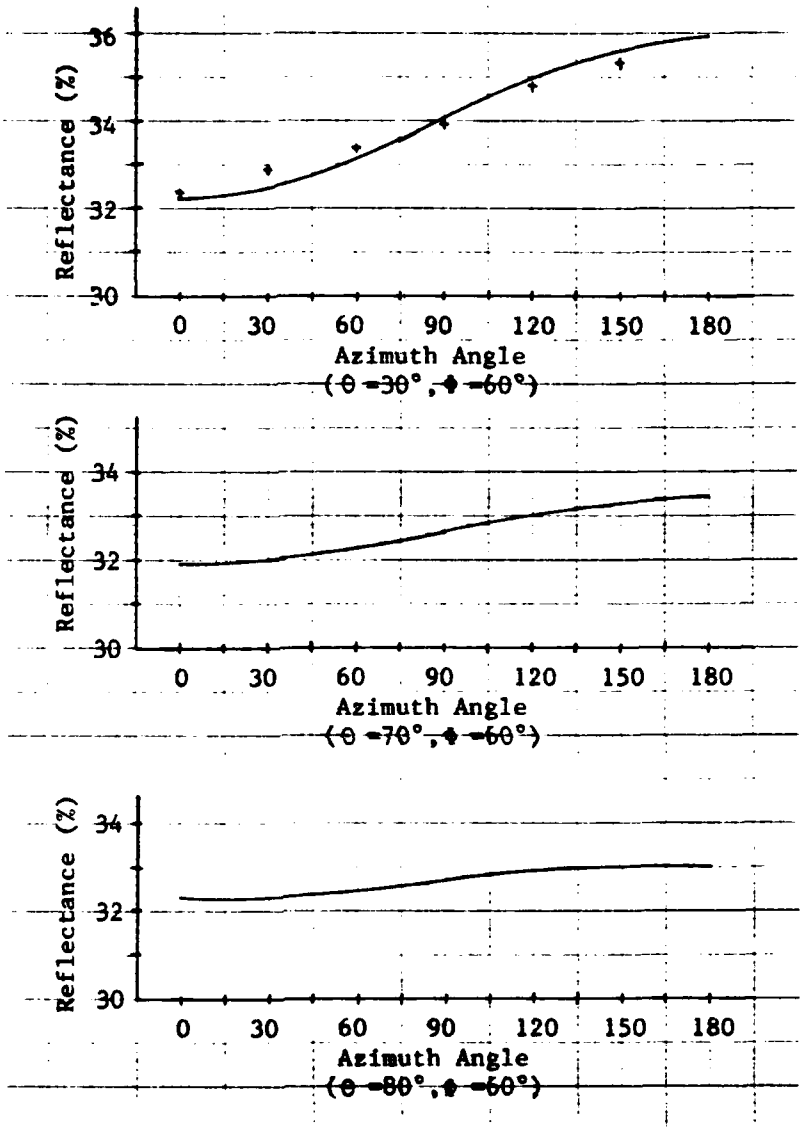

Plots of Specular Reflectance Versus Azimuth Angle

Figure 31

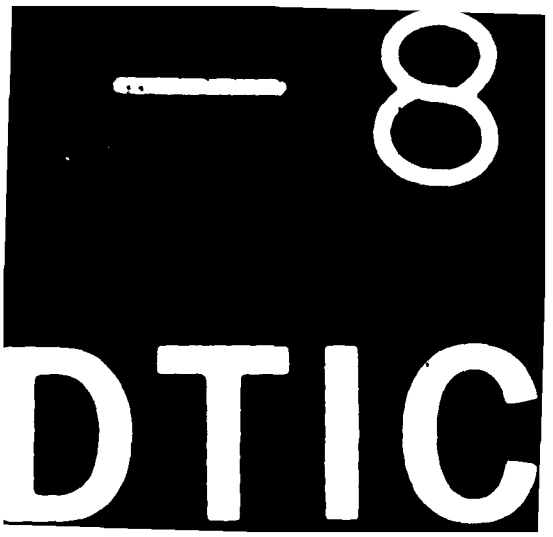
8
DTIC